




Chair of Energy Network Technology

Master's Thesis



Oxygen provision for a steel mill via
flexible electrolyser operation

Stefan Wallner, BSc

May 2022



EIDESSTATTLICHE ERKLÄRUNG

Ich erkläre an Eides statt, dass ich diese Arbeit selbständig verfasst, andere als die angegebenen Quellen und Hilfsmittel nicht benutzt, und mich auch sonst keiner unerlaubten Hilfsmittel bedient habe.

Ich erkläre, dass ich die Richtlinien des Senats der Montanuniversität Leoben zu "Gute wissenschaftliche Praxis" gelesen, verstanden und befolgt habe.

Weiters erkläre ich, dass die elektronische und gedruckte Version der eingereichten wissenschaftlichen Abschlussarbeit formal und inhaltlich identisch sind.

Datum 10.05.2022

A handwritten signature in blue ink, appearing to read 'Stefan Wallner', written over a horizontal line.

Unterschrift Verfasser/in
Stefan Wallner

ABSTRACT

Due to the lower energy consumption and carbon dioxide emissions, steel production via electric arc furnaces represents a promising alternative to integrated steel production via blast furnace and basic oxygen furnace. Nevertheless, steelmaking through the electric arc furnace route consumes high amounts of electric energy, natural gas and oxygen. This thesis deals with feasible ways to provide carbon dioxide neutral oxygen while also cutting back on natural gas demands via the implementation of a power-to-gas plant.

Hydrogen produced by electrolysis could be used to substitute natural gas, either directly by combusting hydrogen or by creating synthetic natural gas via methanation, whereas by-product oxygen could be utilized in the steelmaking process. Moreover, electrolysis would provide a flexibility option, enabling better integration of intermittent energies into the electricity grid and the optimal exploitation of varying electricity prices.

Using an energy system model of a steel mill, different scenarios for the application of electrolysis and subsequent methanation are studied. Then, the flexibility and the economic feasibility of these scenarios are assessed. It turns out that economic performance mainly depends on the utilization of hydrogen. Using technical parameters and prices from 2020, only scenarios focusing on selling hydrogen are profitable, while scenarios focusing on substituting natural gas are not viable under the specified conditions.

KURZFASSUNG

Aufgrund des geringeren Energieverbrauchs und CO₂-Ausstoßes stellt die Stahlproduktion mittels Elektrolichtbogenofen eine vielversprechende Alternative zur Produktion in einem integrierten Stahlwerk durch Hochofen und Konverter dar. Dennoch verursacht das Elektrostahlverfahren nicht nur einen hohen Strombedarf, sondern auch einen hohen Bedarf an Erdgas und Sauerstoff. Diese Arbeit untersucht verschiedene Methoden zur klimaneutralen Bereitstellung von Sauerstoff bei gleichzeitiger Reduktion des Erdgasbedarfs mittels Implementierung einer Power-to-Gas Anlage.

Durch Elektrolyse erzeugter Wasserstoff kann zur Substituierung von Erdgas genutzt werden, entweder direkt durch die Verbrennung von Wasserstoff oder durch die Herstellung von synthetischem Erdgas mittels Methanisierung. Dabei als Nebenprodukt anfallender Sauerstoff kann zur Versorgung des Stahlwerks herangezogen werden. Zudem liefert die Elektrolyse eine Flexibilitätsoption, wodurch eine bessere Integration von erneuerbaren Energiequellen ins Stromnetz und eine optimalere Nutzung variierender Strompreise ermöglicht wird.

Mithilfe eines Modelles für das Energiesystems eines Stahlwerks werden verschiedene Szenarien für den Einsatz von Elektrolyse und Methanisierung in der Stahlproduktion untersucht. Anschließend werden die Flexibilität und die Wirtschaftlichkeit dieser Szenarien analysiert. Wie sich herausstellt, hängt die Rentabilität hauptsächlich von der Nutzung des Wasserstoffes ab. Unter Verwendung von technischen Daten und Preisen aus 2020 erzielen nur solche Szenarien, die sich auf den Verkauf von Wasserstoff fokussieren, wirtschaftliche Erfolge, während sich Szenarien mit Fokus auf die Substituierung von Erdgas unter den betrachteten Bedingungen als unrentabel erweisen.

CONTENTS

Nomenclature	I
List of figures	IV
List of tables	V
1 Introduction	1
2 Task assignment	2
2.1 Research need.....	2
2.2 Research objectives	2
2.3 Methodology.....	3
3 Theoretical Background	4
3.1 Steel production via EAF	4
3.2 Energy efficiency and direct emission reduction measures	6
3.3 Energy demand of the investigated steel mill	7
3.4 Oxygen production	10
3.5 PtG-technologies.....	11
3.5.1 Hydrogen production via steam reforming.....	11
3.5.2 Electrolysis.....	12
3.5.3 Methanation.....	16
4 Model description	18
4.1 Scenario development	18
4.2 Modelling environment	21
4.3 Optimization model	24
4.3.1 Electric energy.....	25
4.3.2 Oxygen.....	26
4.3.3 Hydrogen.....	26
4.3.4 Natural gas	27
4.3.5 Carbon dioxide	28

Contents

4.4 Model for cost calculation	29
4.4.1 Energy cost	29
4.4.2 Capital and operational expenditures.....	31
5 Model parameters	32
5.1 Technical parameters	32
5.2 Capital and operational expenditures	35
5.3 Energy costs	38
6 Results	40
6.1 Optimized supply strategies	40
6.2 Economic assessment	47
6.3 Discussion	51
6.3.1 Demand side management and emission saving potentials.....	51
6.3.2 Economic benefits	52
6.3.3 Sensitivity of the energy system model	52
6.3.4 Model limitations	53
7 Conclusion and outlook.....	54
8 Bibliography	55
9 Appendix	60
9.1 Cost indices	60
9.2 Electricity utilization	60

NOMENCLATURE

Abbreviation

EAF	Electric arc furnace
DR	Direct reduction
BF	Blast furnace
BOF	Basic oxygen furnace
PEMEL	Proton exchange membrane electrolysis
SNG	Synthetic natural gas
PtG	Power-to-gas
LOX	Liquid oxygen
DRI	Direct reduced iron
VD	Vacuum degassing
VOD	Vacuum oxygen decarburization
CCU	Carbon Capture and Utilization
ASU	Air separation unit
PSA	Pressure swing adsorption
SR	Steam reforming
LHV	Lower heating value
HHV	Higher heating value
m_s^3	Standard cubic meter (using 273.15 K and 101 325 Pa)
AEL	Alkaline electrolysis
SOEL	Solid oxide electrolysis
EXAA	Energy Exchange Austria
EIWOG	Elektrizitätswirtschafts- und -organisationsgesetz
EEX	European Energy Exchange AG
CEPCI	Chemical engineering plant cost index

Economic indices

c_{total}	Total annual energy cost [EUR]
c_{energy}	Annual energy cost [EUR]
c_{inv}	Annual investment cost [EUR]
c_{op}	Annual operational cost [EUR]
c_{el}	Annual electricity cost [EUR]
c_{O_2}	Annual oxygen cost [EUR]
c_{NG}	Annual natural gas cost [EUR]
c_{CO_2}	Annual emission allowance cost [EUR]
r_{H_2}	Annual revenue from selling hydrogen [EUR]
EAC	Equivalent annual cost [EUR]
$CAPEX$	Capital expenditure [EUR]
n	Useful asset lifetime [a]
i	Interest rate [-]
$OPEX$	Annual operational expenditure [EUR]
$OPEX_{\%}$	Relative annual operational expenditure [%]
z	Cost capacity exponent [-]
$p_{el,PEMEL}$	Mean purchased electricity price [EUR/MWh _{el}]
$c_{el,PEMEL}$	Annual electricity cost for electrolysis [EUR]

LIST OF FIGURES

Figure 3-1: Flow diagram on various routes of steel production, based on [11]	5
Figure 3-2: Steel production process in the investigated steel mill, based on [9].....	6
Figure 3-3: Overview of the demand model, based on [9]	8
Figure 3-4: Load and generation profiles from the demand model	10
Figure 4-1: Current supply strategy for the steel mill	19
Figure 4-2: Future scenarios for PEMEL implementation in the steel mill	20
Figure 4-3: Example of an energy system model generated via oemof-solph	23
Figure 4-4: Energy system model for optimization.....	25
Figure 4-5: Duration curves for varying electricity prices	30
Figure 5-1: Investment costs for cryogenic storage tanks	36
Figure 5-2: Linearized investment costs for cryogenic storage tanks.....	36
Figure 6-1: Supply strategies for scenario PEMEL 1.....	42
Figure 6-2: Supply strategies for scenario PEMEL 2.....	43
Figure 6-3: Supply strategies for scenario SNG 1	44
Figure 6-4: Supply strategies for scenario SNG 2	45
Figure 6-5: Electricity utilization in scenario PEMEL 2	46
Figure 6-6: Cost structure for future scenarios.....	49
Figure 6-7: Sensitivity of the energy system model to selected parameters	50
Figure 9-1: Electricity utilization in scenario PEMEL 1	61
Figure 9-2: Electricity utilization in scenario PEMEL 2	61
Figure 9-3: Electricity utilization in scenario SNG 1	62
Figure 9-4: Electricity utilization in scenario SNG 2	62

LIST OF TABLES

Table 3-1: Costs for hydrogen production via steam reforming.....	12
Table 3-2: Key performance indicators of electrolysis technologies.....	15
Table 3-3: Costs for hydrogen production via electrolysis.....	16
Table 4-1: Summary of the reference scenario and the future scenarios.....	21
Table 5-1: Technical parameters for production units and storage	33
Table 5-2: Technical parameters for compressors.....	34
Table 5-3: Economic parameters for production units, storage and hydrogen burners.....	37
Table 5-4: Economic parameters for compressors	38
Table 5-5: Prices and framework conditions.....	39
Table 6-1: Indicators for optimized plant layouts.....	41
Table 6-2: Key performance indicators for optimized supply strategies.....	47
Table 6-3: Annual costs for reference case and future scenarios.....	48
Table 9-1: Cost indices for plant costs and production costs	60

1 INTRODUCTION

In 2020, crude steel production in the EU contributed 7.6 % to worldwide production, amounting to 139 million tonnes of steel. Surpassed only by China, this makes the EU the second-largest steel producer in the world and shows the importance of the steel industry in Europe. Steel production using an electric arc furnace (EAF) made up 42.6 % of the total crude steel production in the EU, a share that has remained relatively unchanged since 2011 [1]. Increasing this portion represents a possible way to reduce CO₂ emissions and therefore the environmental impact of the steel industry. Using an EAF for the direct reduction route (DR/EAF), the possible cutback on CO₂ emissions lies in the range of 28-71 % when compared to steel production via blast furnace (BF) and basic oxygen furnace (BOF). Additionally, recycled steel scrap can be used for steel production in an EAF through the secondary process route. In comparison to integrated production, this reduces CO₂ emissions by 63-73 % [2]. Because energy for the EAF process is mostly provided in form of electricity, these values highly depend on the assumed specific CO₂ emissions for electricity generation [3].

Besides electricity, the EAF route also requires natural gas and oxygen as energy sources [2]. By using proton exchange membrane electrolysis (PEMEL) for hydrogen and oxygen production, both demands could be fulfilled in a CO₂-neutral way. While by-product oxygen could be used directly for steel production, hydrogen could be utilized to substitute natural gas or it could be compressed and sold, thus introducing a new source of revenue. As a third option, hydrogen could also be used to produce synthetic natural gas (SNG) through a subsequent methanation process. Moreover, flexible electrolyser operation would allow for optimal utilization of electric energy depending on current electricity availability, electricity prices and product gas demand. This concept, which is referred to as demand side management, brings not only economic benefits but enables the optimal energy usage from renewable and intermittent sources. In view of the upcoming energy transition, a drastic increase in electricity generation from renewable sources is intended and therefore the importance of such flexibility options will also increase [4].

Using the Python framework “oemof”, an energy system model of an EAF steel mill is created. With the help of this model, different scenarios for implementing electrolysis or a combination of electrolysis and methanation are investigated. Afterwards, the costs for providing oxygen and direct fuel to the steel mill are calculated for these scenarios. The technical and economic performance of these scenarios is evaluated by comparison of the results with the status quo.

2 TASK ASSIGNMENT

As mentioned before, the objective of this thesis is to define different scenarios for a more environmentally sustainable provision of oxygen and direct fuel to an EAF steel mill. To accomplish this, a PEMEL system will be implemented into the energy system model. Electrolysis could fulfil the oxygen demand as well as the demand for direct fuel, while also providing demand side flexibility. The following paragraphs describe the research questions of this thesis as well as the applied methodology for answering these questions. Moreover, they provide an overview of existing studies that deal with related tasks.

2.1 Research need

A lot of research has already been done concerning the application of water electrolysis. For example, Gorre et al. [5] and Schiebahn et al. [6] assessed the economic viability of power-to-gas (PtG) technologies, in which hydrogen from electrolysis is utilized either directly or for the production of SNG. They assume different cases with respectively fixed electricity costs and determined the production cost for hydrogen or SNG. An alternative path is shown by van Leeuwen and Mulder [7]. In their work, the revenue from produced hydrogen was assumed and the resulting willingness to pay for electricity was calculated. Kato et al. [8] discussed the potential for reducing the production costs for hydrogen from electrolysis by effectively utilizing by-product oxygen.

All mentioned studies deal with the production of hydrogen or SNG, but utilization potentials for green gases and oxygen in industrial processes receive only a general description. In contrast, the present study uses data from an industry partner to integrate the demand model of an existing steel mill into an optimization model for a PtG-plant. Therefore, the scope of this thesis includes not only the production of hydrogen, oxygen and SNG from electrolysis and methanation but also their demand-actuated utilization in the considered steel mill.

2.2 Research objectives

This thesis focuses on answering the following research questions:

- *How does the implementation of PEMEL and methanation technologies affect demand side management and emission saving potentials of an EAF steel mill?*
- *What economic benefits arise from implementing these technologies and what are the most cost-effective plant layouts and operational strategies?*
- *What variables have the strongest effects on economic viability?*

2.3 Methodology

As mentioned, the energy system used in this thesis consists of a demand model and an optimization model. Dock et al. [9] described a time- and component-resolved energy system of an EAF steel mill, which represents the demand model for this thesis. The optimization model was created using the Python framework “oemof” and describes an energy system for the provision of direct fuel and oxygen, as well as for the utilization and provision of CO₂. A typical “oemof” energy system model consists of different components with specified parameters. By using load profiles from the demand model as parameters for the corresponding components, optimization of the energy system model aims to satisfy all demands of the steel mill in a time-actuated way while minimizing costs.

Manipulation of certain parameters can be used to enable or disable individual components in the energy system, therefore allowing for the definition of different scenarios. Optimization of the energy system model determines then simultaneously the optimal capacities for PtG-plants and storage as well as the optimal operational strategy. When time-resolved and intermittent electricity prices are used as parameters, optimization also aims for efficient and flexible electricity utilization.

The economic viability of the scenarios is assessed based on the total annual energy cost. This value represents the cost for providing oxygen and direct fuel to the steel mill and it contains the annual cost for electricity supplied to the electrolyser, liquid oxygen (LOX), natural gas and CO₂ emission allowances, capital and operational expenditures for implemented equipment as well as revenues generated by hydrogen sales. Contrary to the time-dependent electricity prices, the prices for natural gas, LOX, CO₂ allowances and hydrogen are fixed. Chapter 4.4 describes in more detail how the total energy costs are calculated. The total annual energy costs are then compared to the reference case. This reference case represents the status quo for oxygen and direct fuel provision to the steel mill via purchasing LOX from an external supplier and natural gas from the public gas grid. After listing the total energy costs for all scenarios, the second part of the economic assessment studies the sensitivity of the optimization model to varying parameters. Changes in future performance are identified by altering selected parameters and recording the effect on the total energy costs.

3 THEORETICAL BACKGROUND

The first part of this chapter deals with steelmaking processes and especially with the production process in the investigated steel mill. Moreover, some state-of-research measures for the reduction of direct carbon dioxide emissions of electric steel mills are discussed. Secondly, a model for the energy demand of the investigated steel mill is presented. It is shown that the steel mill consumes large amounts of oxygen, thus the next part of this chapter focuses on oxygen production. Finally, the PtG-technologies studied in this thesis are outlined, starting with electrolysis and proceeding with methanation.

3.1 Steel production via EAF

Steel production processes are distinguished according to the used raw material. Primary steel production uses iron as feedstock, while secondary steel production uses recycled steel scrap [10]. Figure 3-1 shows two possible routes for primary steel production and the process route for secondary steel production via EAF.

Most of the primary steels are produced via the BF/BOF route, which consists of two parts: In the first part, iron ore is reduced to iron in the BF by CO, which is obtained from partially oxidizing coke. The resulting “pig iron” has a high carbon content and contains many impurities. Therefore, iron production needs to be followed up by iron treatment in the BOF. There, oxygen is blown into the melt to reduce the carbon content and to remove impurities, thus transforming pig iron into steel. An alternative path for primary steel production is provided via the DR/EAF route. Instead of coke, DR uses natural gas or coal as a reduction agent, thereby creating direct reduced iron (DRI). Contrary to pig iron, which is not of high enough purity, DRI can be processed to steel in the EAF. The third option for steel production presented in the figure below is the secondary production route or scrap/EAF route. In this process, the EAF is supplied with steel scrap instead of DRI, thus eliminating the need for a reduction agent while also providing a way to recycle steel [10].

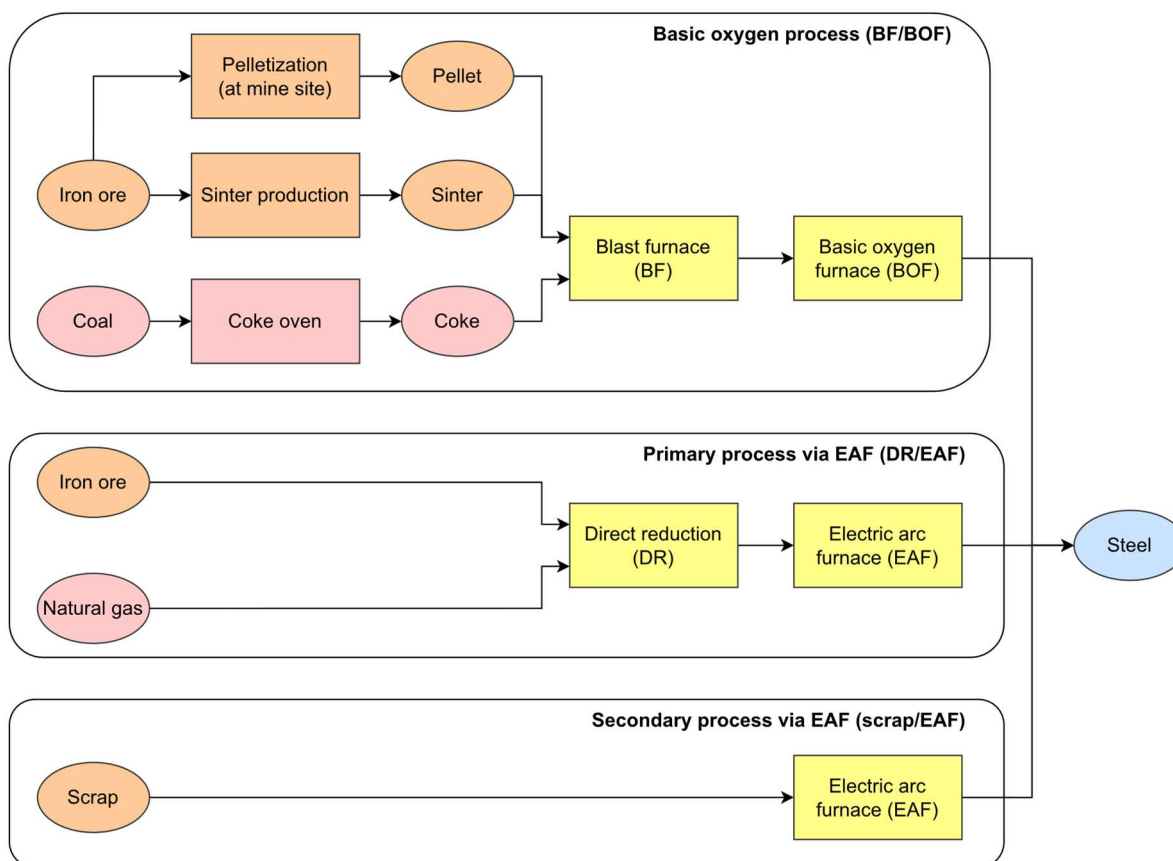


Figure 3-1: Flow diagram on various routes of steel production, based on [11]

The EAF is primarily utilized for the scrap/EAF route, while DRI is mostly just used to supplement steel scrap [10]. The steel mill investigated in the present thesis follows the scrap/EAF route for steel production. Figure 3-2 depicts the processes included in steelmaking for this steel mill. After the EAF is charged with steel scrap, high voltage is applied to the graphite electrodes in the furnace to create an electric arc. At temperatures of up to 3 500 °C, the electric arc is melting the content of the furnace [12]. Many EAFs use natural gas burners for additional energy input, but the EAF in the studied steel mill does not [9]. However, the furnace uses oxygen to obtain energy from chemical reactions and reduce the electric energy demand in this way [13]. A requirement for oxygen also arises from steel refining, when oxygen is blown into the molten steel to oxidize impurities [12]. Moreover, oxygen is injected together with carbon via lances or burners to create CO gas for slag foaming, a process that is important for the protection of the furnace lining but also for its positive effects on heat transfer and arc stability [14].

After melting in the EAF, so-called ladles are used as transport and treatment vessels for the liquid steel. Thus, the following secondary metallurgy processes are also referred to as ladle metallurgy [15]. To remove humidity and avoid excessive temperature gradients, the ladles are preheated to roughly 1 000 °C by natural gas burners before tapping the EAF. In the figure,

this ladle heating process is presented as a supporting process, alongside the operation of the dust extraction system of the steel mill and the process steam boiler [9].

Ladle metallurgy generally aims to remove oxygen, hydrogen, sulfur and undesirable nonmetallic elements, while also enhancing the mechanical properties and improving the microstructure of the steel [15]. The ladle furnace shown in the diagram below is used to adjust the temperature of the steel throughout these processes. In the case of the investigated steel mill, high-alloy and special steels need to be produced, therefore vacuum degassing (VD) and vacuum oxygen decarburization (VOD) is required to remove dissolved gases and reduce the remaining carbon content. Following the ladle metallurgy processes, steel is cast into ingots. The properties of these ingots are then adjusted via heat treatment in an annealing furnace, while empty ladles return to the ladle heaters before renewed deployment [9].

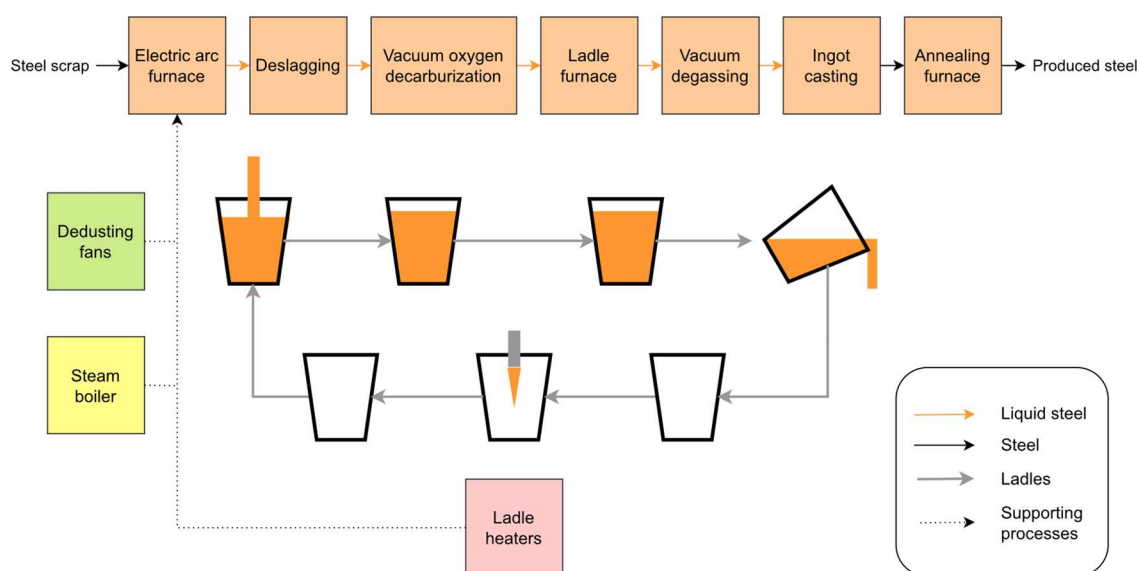


Figure 3-2: Steel production process in the investigated steel mill, based on [9]

To optimize the implementation and operation of PtG-technologies in the steel mill, it is necessary to integrate time-actuated energy demands of the steelmaking process into the energy system model. Some measures to increase energy efficiency and decrease direct CO₂ emissions in the steel mill have already been investigated and are therefore also integrated into the energy system model. Discussing these measures is the aim of the next chapter.

3.2 Energy efficiency and direct emission reduction measures

One measure to increase energy efficiency and decrease emissions in the steel mill is the application of Oxyfuel burners for ladle preheating. The following paragraphs describe these Oxyfuel burners in more detail and point out possible ways to utilize CO₂ obtained from Oxyfuel combustion and subsequent Carbon Capture.

More than half of the natural gas burners for ladle preheating have been replaced by Oxyfuel burners. These Oxyfuel burners use high purity oxygen instead of air for combusting natural gas. Therefore, unnecessary N_2 is eliminated from the oxidizer, which brings many benefits. One of these advantages is increased thermal efficiency because exhaust gas flow rates are lower and thus losses from exhaust gases are reduced. For the same reason, higher flame temperatures and therefore higher rates of heat radiation are achieved, allowing for faster heating and thus increased processing rates. Further benefits include improved flame characteristics due to Oxyfuel combustion [13]. Moreover, a rather big advantage arises from the fact that the flue gas contains CO_2 in high concentrations. Thus, capturing CO_2 from the ladle heater exhaust gas is greatly simplified, introducing a potential for Carbon Capture and Utilization (CCU) [16].

As suggested, CO_2 -intensive flue gases, originating from the Oxyfuel ladle heaters in the considered steel mill, are harnessed via CCU. Dong and Wang [17] list possible applications for captured CO_2 in steel production processes. Another method is the utilization for water treatment, which was investigated by Vansant [18]. Alkaline wastewaters from steelmaking processes such as VD or VOD need to be neutralized before draining into the sewerage. Treatment of such wastewaters with CO_2 is much safer than storing and handling conventionally used acids like sulphuric acid. Moreover, less reagent, equipment, monitoring devices and downtimes are needed while equipment lifetimes increase [18]. However, the potential for water treatment using CO_2 lies not only within neutralizing alkaline wastewater. Carbonation of water provides an inexpensive method for eliminating Ca^{2+} and Mg^{2+} ions, therefore CO_2 can also be utilized to remove hardness from cooling water [19].

To integrate the energy demands of the steel mill as well as the above discussed efficiency and direct emission reduction measures into the energy system model, an already existing model for the steel mills time- and -component resolved energy demands is used. The following chapter describes this demand model.

3.3 Energy demand of the investigated steel mill

In their study, Dock et al. [9] described an energy system model of the investigated EAF steel mill. They identified different sub-components of the energy system and generated load profiles for the time-resolved energy demands of these components by using data from an existing steel mill. Thereby, they applied various modelling approaches depending on the operation characteristics of the sub-components. For instance, they used stochastic modelling to determine process parameters and Markov chains to generate synthetic load and generation profiles. As a result, Dock et al. created a time- and component-resolved model of

the overall energy system considering demand profiles for electricity, process steam, natural gas, oxygen, CO₂ as well as waste heat and flue gas flows [9].

This thesis uses a slightly simplified version of the steel mill model which focuses only on natural gas, oxygen and CO₂. While the optimization model incorporates the electricity demand for electrolysis and gas compression, the electricity demand of the steel mill itself is disregarded because it is independent of the scenario selection. Waste heat flows are also not considered because the treatment of heat flows lies outside of the scope of this thesis. Figure 3-3 depicts the demand model and shows the different sub-components, which represent the main process steps and auxiliary processes in the investigated steel mill. Oxygen is used in the EAF and for vacuum treatment via VOD. Furthermore, Oxyfuel heaters are supplied with oxygen. VOD and VD treatments require process steam generated by combusting natural gas in the steam boiler. Instead of considering these steam demand profiles, only the resulting natural gas demand of the steam boiler is regarded and translated to a natural gas demand for vacuum treatments. Additional natural gas consumers are the annealing furnace and the ladle heaters. Applying Oxyfuel burners for ladle heating enables subsequent CCU, thus the respective ladle heaters represent a CO₂ source. According to subchapter 3.2, CO₂ is then used for water treatment. Depending on the current load and generation there can either be a CO₂ surplus or a CO₂ shortage.

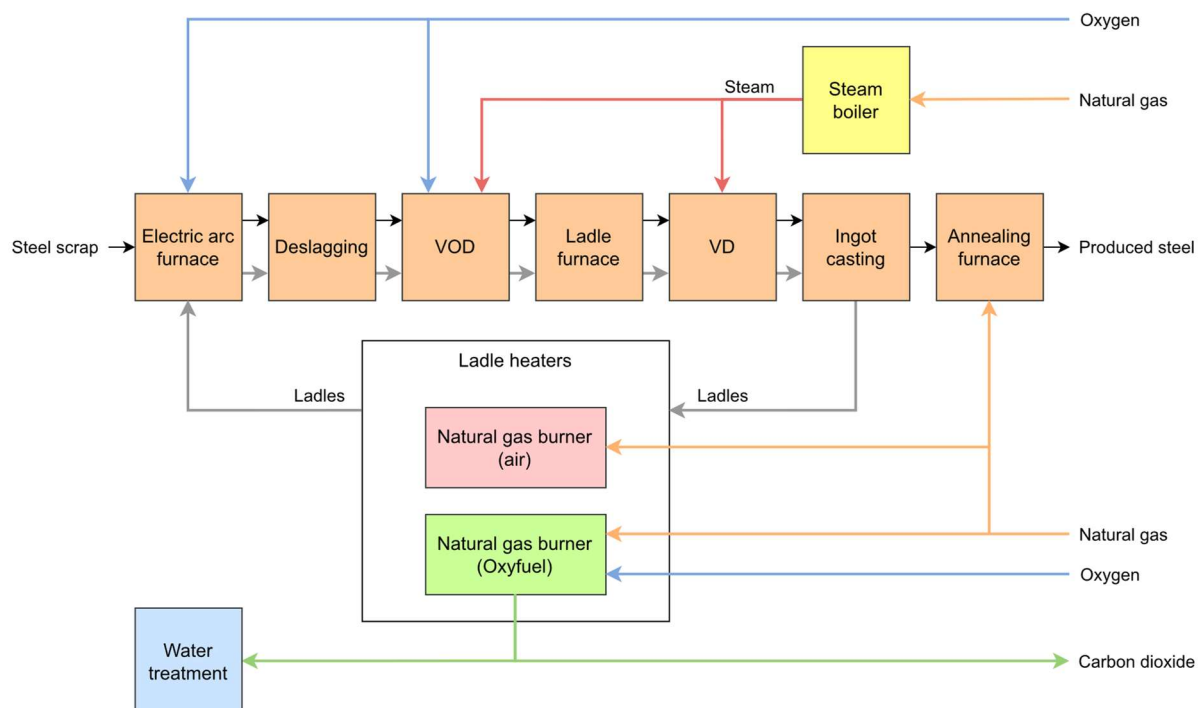


Figure 3-3: Overview of the demand model, based on [9]

The time-resolved load and generation profiles for oxygen, natural gas and CO₂ all span four weeks with a resolution of 15 min. For clear representation, Figure 3-4 shows only the first

week of these profiles, beginning with Sunday and ending with Saturday. The actual load and generation values in kg/min for oxygen and CO₂ or in kW_{NG, HHV} for natural gas are normalized using the respective maximum load. Descriptions are added to the diagrams to declare which sub-components of the demand model contribute to certain parts of the profiles. Starting with oxygen, only a small load is needed to supply the ladle heaters during the weekend. These values increase over the weekdays, creating an oxygen demand basis. Greater divergences from this basis stem from the comparatively high EAF demands. Further oxygen consumers are the sub-component for VOD treatment and a small non-assigned baseload, which combines the remaining consumers. A certain baseload value also exists for natural gas, depicted by the dotted line in the figure. Analogous to the oxygen load, ladle heating generates a small natural gas demand during weekends. The overall curvature of the natural gas load is due to the annealing furnace demand, while the natural gas demands for ladle heating and vacuum treatments generate deviations from this curve. Contrary to the diagram for oxygen and natural gas, there exist two flow profiles for CO₂. The solid line represents the CO₂ demand for water treatment, while the dashed line portrays the possible CO₂ generation from CCU after ladle heating via Oxyfuel combustion. Both profiles are normalized using the maximum demand value for water treatment.

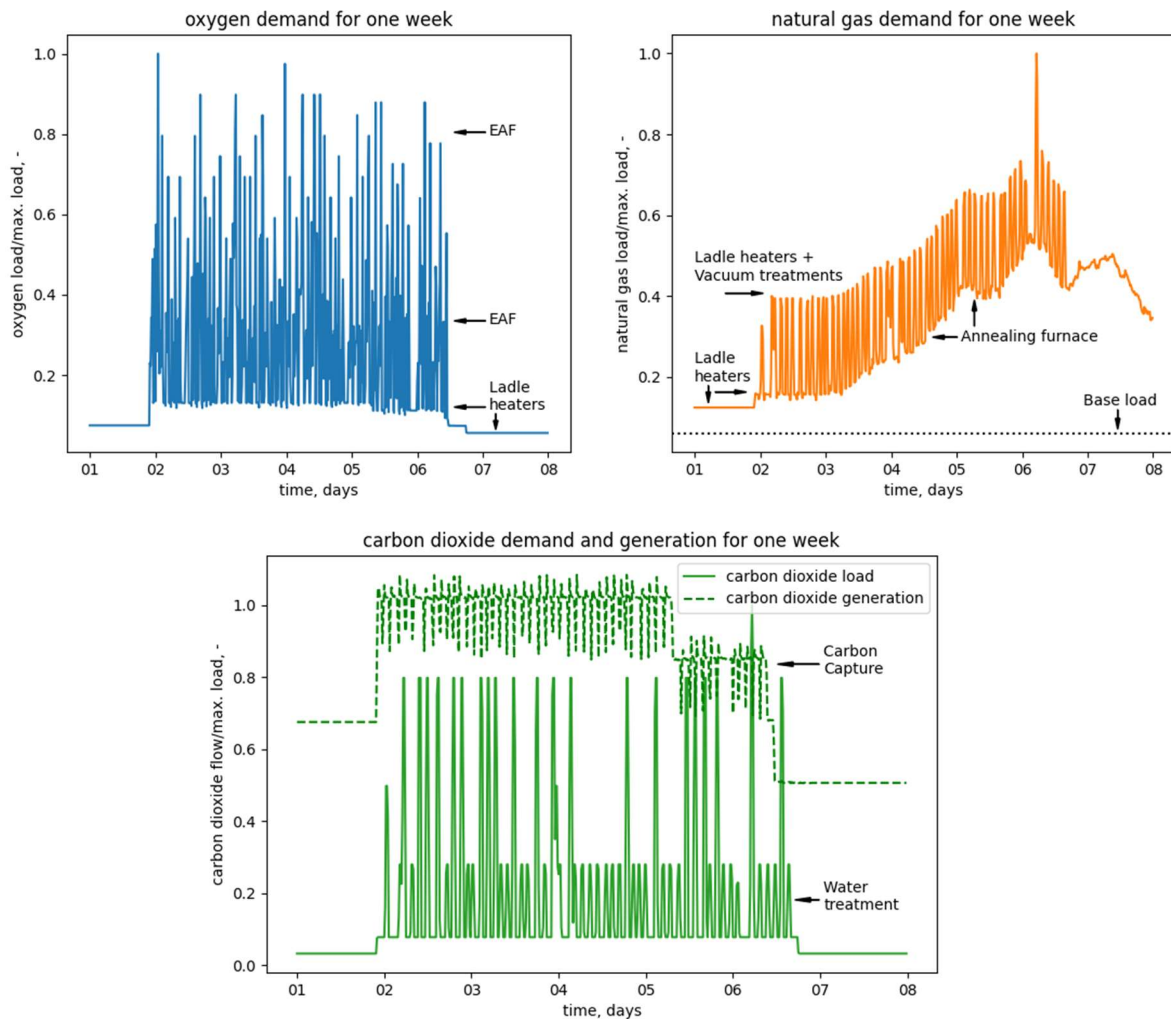


Figure 3-4: Load and generation profiles from the demand model

As can be seen from Figure 3-4, steelmaking via EAF consumes large amounts of oxygen, while a significant oxygen demand also arises from Oxyfuel ladle heating. The following chapter deals therefore with different methods for providing the necessary oxygen. Firstly, conventional methods for oxygen production are introduced. The energy demand for these production methods is then compared to the energy demand for generating oxygen through electrolysis.

3.4 Oxygen production

Currently, cryogenic air separation via air separation unit (ASU) is the conventional method for large-scale and high purity oxygen production. After compression and pre-treatment, the air is separated by fractional distillation, thereby producing oxygen, nitrogen and argon either in liquid or in gaseous form. Cryogenic distillation is cost-effective when large quantities of oxygen are needed but it is not suitable for smaller-scale production. Oxygen for plants with smaller demands is usually provided by delivery from a centralized ASU or by on-site production using an adsorption process. In adsorption processes, the ability of some

materials, such as zeolites, to adsorb nitrogen is utilized to filter air, thus producing an oxygen stream with purities typically in the range between 93-95 %_{vol}. In comparison, an ASU produces oxygen with purities higher than 99 %_{vol}. Periodically, the adsorbent needs to be regenerated. Pressure swing adsorption (PSA) accomplishes this by pressure reduction [8]. The specific energy consumption for oxygen production for both technologies, cryogenic distillation and PSA, are about 0.5 kWh_{el}/m_s³ [8].

Implementing and operating an electrolyser provides an alternative oxygen source. In chapter 3.5.2, the electrolysis process is described, while typical efficiencies for PEMEL systems are listed in Table 3-2. Using the efficiencies cited by Carmo et al. [20], the specific energy consumption for generating oxygen from electricity is calculated to be in the range between 9.0 and 15 kWh_{el}/m_s³. This shows that oxygen production by electrolysis is much more energy-intensive than conventional production. Electrolysis operation should therefore focus on cost-effective hydrogen utilization, while oxygen represents a by-product. The production cost for hydrogen could then be lowered by utilizing both hydrogen and oxygen [8].

Alongside the high oxygen demand, the energy demand model of the steel mill also includes a large demand for natural gas. An electrolyser could partially supply this natural gas demand either by using hydrogen as direct fuel or by producing SNG from hydrogen. Thus, a potential for utilizing hydrogen alongside oxygen already exists in the steel mill. The following paragraphs are therefore dedicated to hydrogen production and SNG production via PtG-technologies.

3.5 PtG-technologies

For later comparison with electrolysis, the conventional hydrogen production process via steam reforming (SR) is described and cited production costs for this method are listed. Afterwards, the actual PtG-technologies are introduced, starting with common electrolysis technologies. The last part of this chapter deals with the production of SNG via methanation.

3.5.1 Hydrogen production via steam reforming

Presently, SR represents the most developed technology for industrial-scale hydrogen production. A variety of gases containing hydrocarbon can be used for feedstock, such as pure methane or natural gas. SR produces hydrogen and carbon oxides through catalytic conversion of hydrocarbons and steam. Following the reforming step, the product gas is supplied to a water-gas shift reactor where CO reacts with steam to produce even more hydrogen, leaving mainly hydrogen and CO₂ in the product gas. These gases are then separated from each other through a CO₂-removal process or by PSA, thus creating a high purity hydrogen stream [21].

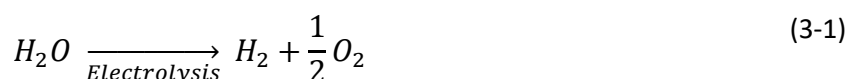
Table 3-1 lists cited costs for the production of hydrogen via SR. These production costs highly depend on the costs for feedstock gases. Nikolaidis and Poullikkas [21] estimated specific costs for hydrogen production with and without additional Carbon Capture and Sequestration for 2015. They assumed a natural gas price of 10 USD/MMBtu, corresponding to approximately 31 EUR/MWh_{NG, HHV} in 2020. The natural gas price and the resulting hydrogen production costs are adjusted to 2020 EUR by using cost indices listed in section 9.1. Lemus and Duart [22] showed linear dependencies of fossil fuel prices and SR hydrogen production costs. Using again a natural gas price of 31 EUR/MWh_{NG, HHV}, hydrogen production cost value about 2.00 EUR/kg_{H₂}. Because the SR process needs natural gas for feedstock, thereby generated hydrogen is often referred to as “grey hydrogen”. In contrast, “green hydrogen” is produced via electrolysis and by utilizing only CO₂-neutral energy sources [23].

Table 3-1: Costs for hydrogen production via steam reforming

Specific production cost	Unit	Reference
<i>with Carbon Capture</i>		
2.04	EUR/kg _{H₂}	Nikolaidis and Poullikkas [21]
<i>without Carbon Capture</i>		
1.87	EUR/kg _{H₂}	Nikolaidis and Poullikkas [21]
2.00	EUR/kg _{H₂}	Lemus and Duart [22]

3.5.2 Electrolysis

An electrolyser produces hydrogen and oxygen by electrochemically splitting water molecules. Due to the stoichiometry of this splitting reaction, the volume of by-product oxygen equals half of the hydrogen volume. Equation (3-1) describes the overall reaction for water splitting via electrolysis [24]:



Water splitting is a process that needs to be supplied with energy. This energy comes in the form of electricity. However, a part of the energy can be substituted by providing thermal energy. The efficiency of an electrolyser is calculated by dividing the enthalpy of the produced hydrogen by the energy demand for electrolysis. When such efficiencies are stated, it is important to mention if the hydrogen enthalpy is based on the lower heating value (LHV) or the higher heating value (HHV) of hydrogen [24]. The optimization model uses the HHV

efficiency for electrolysis, therefore Formula (3-2) shows how the adequate electrolyser efficiency ($\eta_{el,HHV}$) is defined. \dot{V}_{H_2} is the volume flow of produced hydrogen assuming standard physical conditions in m_s^3/h , HHV_{H_2} is the higher heating value of hydrogen in kWh/m_s^3 and P_{el} is the electric power consumed by the electrolyser in kW_{el} [24].

$$\eta_{el,HHV} = \frac{\dot{V}_{H_2} HHV_{H_2}}{P_{el}} \quad (3-2)$$

Most water electrolysis is carried out by three main technologies: Alkaline electrolysis (AEL), proton exchange membrane electrolysis (PEMEL) and solid oxide electrolysis (SOEL) [24]. The mentioned electrolysis technologies are illustrated in the following section of the thesis. Subsequently, some key performance indicators of AEL and PEMEL as well as cited costs for the production of hydrogen via electrolysis are presented.

3.5.2.1 Alkaline electrolysis

In a discussion of electrolysis technologies, alkaline electrolysis (AEL) represents a good starting point because of its technological maturity. Thanks to their availability for large-scale implementation and their cost-effectiveness due to relatively cheap electrode materials, alkaline electrolysers dominate the nowadays market for electrochemical hydrogen production [25]. The electrolyser contains a liquid electrolyte, typically a 25-30 % aqueous KOH solution. This electrolyte is circulated between the electrolyser, where it is brought into contact with the electrodes, and two drums for storage of the liquid as well as for the removal of the product gases, respectively hydrogen or oxygen. Meanwhile, a diaphragm guarantees the separation of the two electrodes [24]. As mentioned, electrodes for AEL consist of non-expensive materials, for instance, iron and nickel [25].

Although AEL is a mature technology, major issues remain. Firstly, product gases can diffuse through the diaphragm. This means that oxygen can cross this barrier and react back to water in the presence of hydrogen, thus reducing the efficiency. Moreover, diffusing hydrogen can mix with the oxygen product flow. This issue intensifies at a low load of under 40 %_{nom} of nominal load when oxygen production rates decrease. Hydrogen concentrations could then increase to potentially hazardous levels, which is why only low partial load changes can be achieved with AEL [20]. The resulting minimum load for AEL operation of course heavily restricts the usability as a flexibility option. Buttler and Spliethoff [24] cite a minimal load between 10-40 %_{nom}. However, according to them, minimal loads for most commercial electrolysers fall in the range between 20 and 25 %_{nom}. Other disadvantages of AEL are low maximum current densities and the inability to function at high pressures [20].

3.5.2.2 *Proton exchange membrane electrolysis*

Proton exchange membrane electrolysis or polymer electrolyte membrane electrolysis (PEMEL) represents an alternative to alkaline electrolysis. The eponymous component for this type of technology is the proton exchange membrane, consisting of a perfluorosulfonic acid polymer [26]. Because this membrane creates a corrosive acidic environment, only a small variety of expensive materials can be used for PEMEL. For instance, catalysts consist of noble metals such as Pt, Ir and Ru, while titanium-based materials are used for current collectors and separation plates [20].

Thanks to higher achievable maximum current densities, proton exchange membrane electrolyser designs are more compact compared to alkaline electrolysers. Further advantages concern the flexible operation of the electrolyser. PEMEL offers shorter cold start-up times and the electrolyser load can be varied over the full load range. Although AEL is still regarded as the more mature technology, PEMEL systems already range up to the MW scale [24]. Another benefit regarding PEMEL compared to AEL is a greater potential for cost reduction with increasing capacity. Therefore, the gap between PEMEL and AEL investment costs is shrinking for large scale production [27]. Due to the listed benefits, this thesis deals with the implementation of PEMEL instead of AEL.

3.5.2.3 *Solid oxide electrolysis*

An electrolysis technology that has recently attracted more attention is solid oxide electrolysis (SOEL). The operating temperatures for SOEL lie in the range between 700 and 900 °C. On the one hand, SOEL exceeds both AEL and PEMEL in efficiency due to these high temperatures. On the other hand, working with such temperatures provides a great challenge for material stability. Preheated steam enters as feed into the SOEL stack, while oxygen and a mixture of steam and hydrogen leave. Air can optionally be used to remove oxygen. This hurts the efficiency of the electrolyser but averts potential problems from handling pure oxygen at high temperatures. The hot steam-hydrogen product stream is utilized for preheating the feed stream in a recuperator before hydrogen is separated via cooling and condensing of water. In addition to preheating and evaporating in a recuperator, the input steam also needs to be superheated by an external heat source or by an electric heater to reach the SOEL inlet temperature [24].

SOEL shows some interesting advantages, especially for power-to-liquid or power-to-gas applications. For instance, subsequent exothermic processes such as the production of methanol or SNG can be utilized to provide SOEL with heat. Moreover, SOEL can electrolyze CO₂ alongside steam, therefore creating a hydrogen and CO mixture which would simplify potential downstream synthesis operations. Another important feature of SOEL is its ability to

change flexibly from electrolysis mode to fuel cell mode. These listed advantages could allow for interesting applications of SOEL in the future. But nowadays, this technology is still at the research level, therefore it is not further regarded in this thesis [24].

3.5.2.4 Key performance indicators and hydrogen production costs

In Table 3-2, efficiencies and specific investment costs for AEL and PEMEL systems are listed. All system efficiencies are based on the HHV of hydrogen and include energy consumption for rectifiers and utilities but exclude external compression. The specific investment costs represent the investment cost for an electrolyser per kW of electricity input capacity. Therefore, specific investment costs are given in EUR/kW_{el}. All monetary values are adjusted to 2020 EUR by using the cost indices depicted in section 9.1.

Table 3-2: Key performance indicators of electrolysis technologies

KPI	Unit	AEL	PEMEL	Reference
system efficiency	% _{HHV}	60-71	54-71	[24]
	% _{HHV}	70-80	-	[8]
	% _{HHV}	75	-	[5]
	% _{HHV}	-	64	[27]
	% _{HHV}	-	47-79	[20]
specific investment costs	EUR/kW _{el}	791-1 480	1 480-2 470	[24]
	EUR/kW _{el}	558	> 1 120	[8]
	EUR/kW _{el}	650	-	[5]

Table 3-3 shows different cost ranges for hydrogen production via electrolysis. Yu et al. [23] cite production costs for Europe. Nikolaidis and Poullikkas [21] give hydrogen production costs depending on different energy sources for electrolysis. Kuckshinrichs et al. [28] calculated hydrogen costs for AEL sites in Germany, Austria and Spain. They give the German production cost and state that the costs for Austria and Spain are about 15-18 % higher. Thus, hydrogen production costs for Austria are calculated. Analogous to the SR production costs and the specific electrolyser costs, all values are given in 2020 EUR by utilizing the cost indices from section 9.1. When comparing the electrolysis hydrogen production costs and the SR production costs from Table 3-1, it can be seen that the costs for hydrogen from SR are generally lower. Therefore, SR is still regarded as the most cost-effective production method for hydrogen [21].

Table 3-3: Costs for hydrogen production via electrolysis

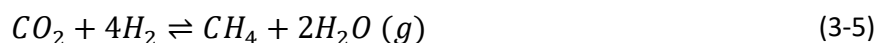
Specific production cost	Unit	Reference
1.96-6.86	EUR/kg _{H2}	Yu et al. [23]
3.74-9.44	EUR/kg _{H2}	Nikolaidis and Poullikkas [21]
4.30-4.42	EUR/kg _{H2}	Kuckshinrichs et al. [28]

3.5.3 Methanation

One possibility to utilize hydrogen from electrolysis comes in the form of methanation. Methanation is a chemical process that converts hydrogen and either CO or CO₂ to CH₄ which can then be used as SNG. Thus, CO-methanation and CO₂-methanation can be distinguished [29]. Due to the existing CCU potential of the steel mill described in section 3.2, this thesis focuses on CO₂-methanation. Thereby, the two reactions stated below are of importance. Equation (3-3) depicts the process of CO-methanation, which also contributes to CO₂-methanation. Equation (3-4) represents the reverse water-gas shift reaction. This reaction allows for the conversion of CO₂ to CO, therefore enabling the methanation of CO₂ [29].



CO-methanation is an exothermic reaction, while the reverse water-gas shift reaction is endothermic. Therefore, the combined reaction for CO₂-methanation is less exothermic than exclusive CO-methanation. Equation (3-5) shows the complete reaction for the methanation of CO₂ [29].



Mutz et al. [30] studied the methanation of CO₂ with a commercial Ni-based catalyst. They found a CO₂ conversion rate of 81 % and a selectivity towards CH₄ of 99 % at 400 °C. Using these values and the HHVs of hydrogen and CH₄, the HHV based methanation efficiency can be calculated. The resulting efficiency of 62 %_{HHV} means that 62 % of the energy input in form of hydrogen enthalpy is converted to CH₄ enthalpy. Gorre et al. [5] state investment costs for methanation, depending on the HHV based CH₄ power output, with 450 EUR/kW_{CH₄, HHV} in 2020. Thereby, they assumed a maximum load change rate of 3 %_{nom}/min in per cent of nominal power to keep the quality of product gas constant. According to Specht et al. [31],

operation in a load range between 70 and 100 %_{nom} also guarantees that there are no significant influences on product gas quality.

After describing the processes for electrolysis and methanation as well as listing important key performance indicators, adding these PtG-technologies to the energy system model represents the next step towards a complete optimization model. Therefore, the following chapter aims to develop different scenarios for integrating a PtG-plant into the investigated steel mill.

4 MODEL DESCRIPTION

The first objective of this chapter is to describe the different scenarios for the supply of energy carriers and gases, including the status quo as well as the implementation of PtG-technologies. To identify optimal plant layouts and operational strategies for these scenarios, an energy system model is used. Thus, the modelling environment and the energy system model are presented in the next part of this chapter. Finally, the cost model for the economic assessment of all scenarios is presented.

4.1 Scenario development

Figure 4-1 depicts the current situation for the demand-actuated provision of oxygen and natural gas. Oxygen for the steel mill is purchased from a centralized large-scale ASU and is delivered in liquid form via tank trucks. In the figure, this is represented by the component “LOX delivery”. It is assumed that thereby obtained LOX is then stored in a cryogenic tank. Oxygen from LOX storage is then vaporized prior to its utilization in the steel mill. Costs for delivery of LOX arise from purchasing the oxygen itself and from transportation. Due to its proximity to a natural gas pipeline, the steel mill is easily supplied with natural gas. Purchase of natural gas from the gas line is represented by the “gas grid” component and creates costs depending on the natural gas price and the allowance price for resulting CO₂ emissions. The CO₂ generation potential from CCU is assumed to be utilized for water treatment. Possible surplus CO₂ is not captured but rather exhausted as flue gas. For further utilization or storage in a pressurized tank, captured CO₂ is compressed, resulting in electricity costs and investment costs for the compressor. Moreover, investment costs for storage tanks for oxygen and CO₂ are considered as well as expenditures for the storage operation. The described scenario forms the reference scenario for the future scenarios.

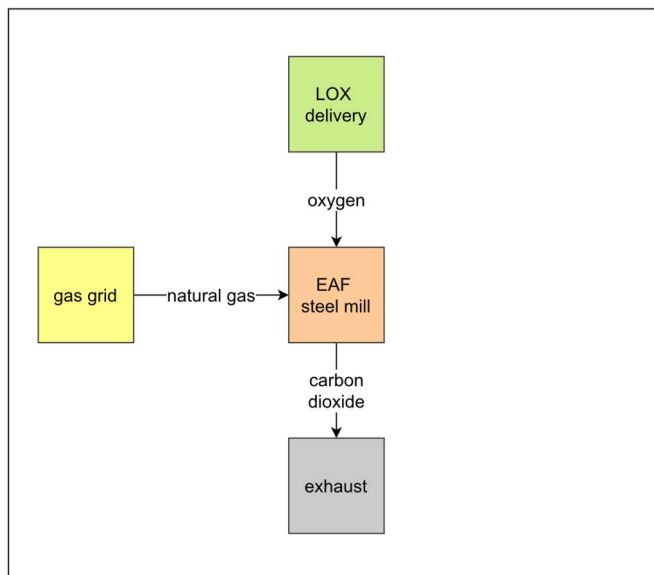


Figure 4-1: Current supply strategy for the steel mill

Four future scenarios for supplying the steel mill demands via PEMEL were selected for subsequent optimization and investigation of their economic feasibility. Figure 4-2 shows these scenarios. The first two scenarios only consider implementing PEMEL, while scenarios SNG 1 and SNG 2 consider a combination of PEMEL and methanation.

- Scenario PEMEL 1:** In the first future scenario, some of the natural gas burners for ladle heating are converted to hydrogen burners. Necessary hydrogen is then provided via PEMEL, therefore reducing natural gas demand and CO₂ emissions. However, only part of the ladle heaters can be converted because otherwise not enough CO₂ would be generated by CCU to cover the water treatment demand. The amount of by-product oxygen arising from hydrogen production via PEMEL is not high enough to supply the steel mill demand all alone. Nevertheless, the demand for LOX from external suppliers is reduced. As mentioned before, oxygen is stored in liquid form in the reference scenario. However, in scenarios with additional provision of gaseous oxygen via electrolysis, implementing a cryogenic storage for LOX would require either a liquification process for on-site generated oxygen or two separate tanks for liquid and gaseous storage. Thus, it is assumed that externally supplied LOX is vaporized before storage in a pressurized gas tank.
- Scenario PEMEL 2:** In the first scenario, the electrolyser focuses on supplying a certain hydrogen demand. Contrary, PEMEL is used in the second scenario to cover the complete oxygen demand of the steel mill, thereby also generating large amounts of hydrogen. Hydrogen is then compressed for subsequent transportation and sold off, assuming a fixed and reasonable price for green hydrogen.

Model description

- Scenario SNG 1:** This scenario deals with a combination of electrolysis and methanation. The complete CCU potential from Oxyfuel ladle heating is utilized, thus generating more CO₂ than necessary for water treatment. This CO₂ surplus is then used for SNG production via methanation. By combusting SNG, the natural gas demand of the steel mill is reduced, while a hydrogen demand arises from methanation. Analogous to the first scenario, an electrolyser is used for supplying hydrogen and for generating by-product oxygen, thereby reducing the LOX demand.
- Scenario SNG 2:** This scenario is similar to the previous one because again the complete CCU potential of the steel mill is utilized for the production of SNG. However, in this scenario PEMEL focuses on covering the oxygen demand of the steel mill, thus producing more hydrogen than needed for methanation. Surplus hydrogen is then compressed and sold off.

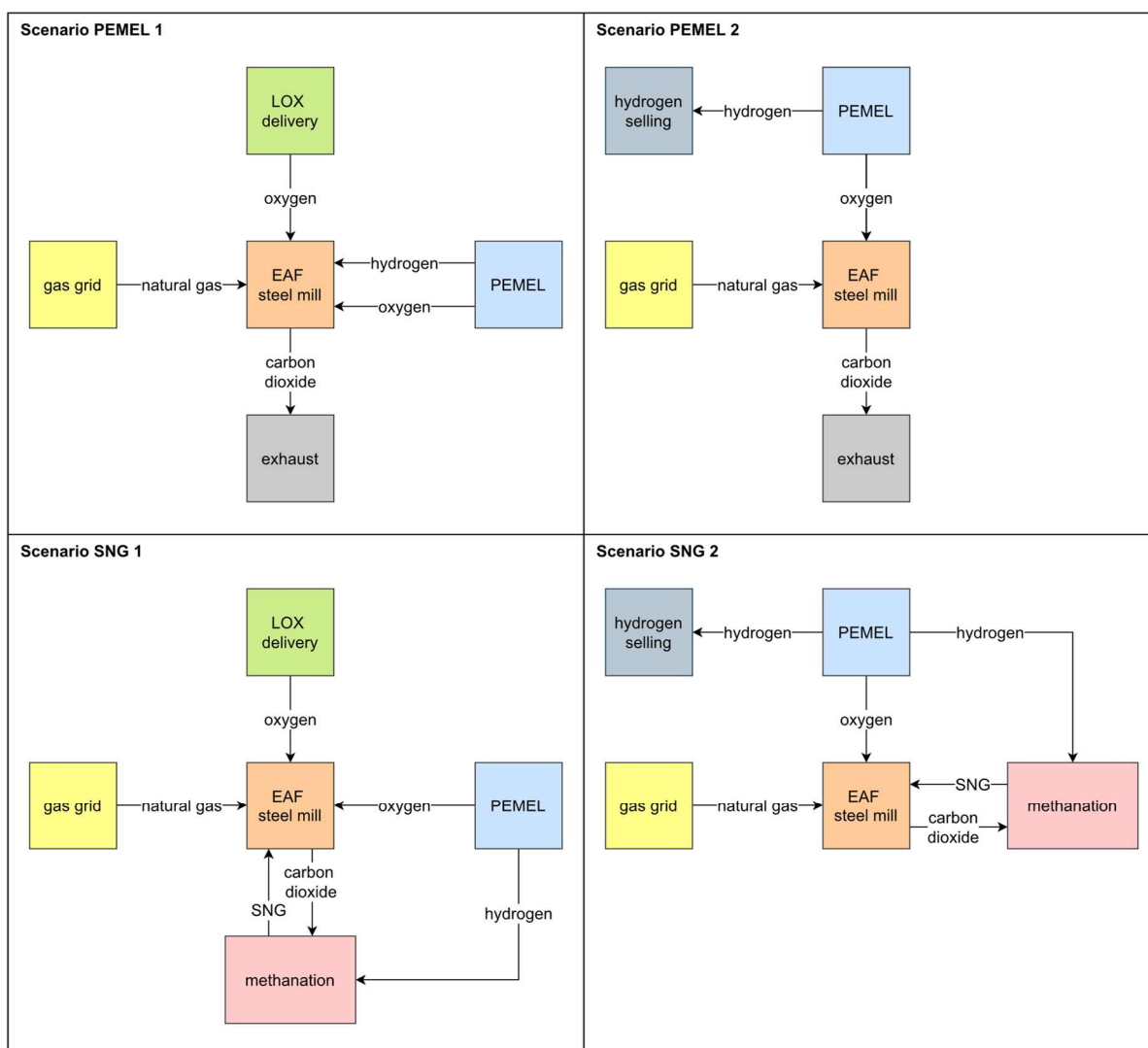


Figure 4-2: Future scenarios for PEMEL implementation in the steel mill

Table 4-1 summarizes the status quo or reference scenario and the considered future scenarios. For every scenario the methods for oxygen provision and hydrogen utilization as well as the necessary storage tanks and compressors are listed. In the reference scenario, oxygen storage is referred to as LOX storage, indicating that oxygen is stored in a cryogenic tank, while all the other storage units represent pressurized gas tanks.

Table 4-1: Summary of the reference scenario and the future scenarios

	Reference	PEMEL 1	PEMEL 2	SNG 1	SNG 2
oxygen supply	delivery	delivery, electrolysis	electrolysis	delivery, electrolysis	electrolysis
hydrogen utilization	-	direct fuel	selling	methanation	methanation, selling
storage tanks	LOX, CO ₂	oxygen, CO ₂ , hydrogen	oxygen, CO ₂	oxygen, CO ₂	oxygen, CO ₂
compressors	CO ₂	CO ₂	CO ₂ , hydrogen	CO ₂	CO ₂ , hydrogen

To model and optimize the presented scenarios, an energy system model is needed. Therefore, the purpose of the next chapter is to introduce the Python toolbox used for modelling. Subsequently, the actual model of the energy system and its components are described.

4.2 Modelling environment

For creating the energy system model, the Python toolbox “oemof”, short for “Open Energy Modelling Framework”, is used. Oemof provides a loose organisational framework for different energy system modelling tools. Therefore, oemof consists of various projects, of which “oemof-solph” or Solph is mainly used in the present thesis [32].

Solph together with an appropriate solver allows for modelling and optimization of energy systems. The first step in creating an energy system model is commonly the generation of an energy system object with a defined time range and a defined time resolution. An energy system contains classes, which are further divided into nodes and edges. Nodes are used as the main building blocks for the energy system, while edges connect these nodes and represent flows, such as mass flows or energy flows. Figure 4-3 shows an exemplary energy system model to better illustrate the thereby applied classes [33].

There are two different types of nodes, components and buses. Buses represent balanced grids, for instance, an electricity grid or a grid for mass flows. All components which are part

of a grid are connected to the respective bus object via flows. The overall sum of all outflows and inflows of one bus object has then to equal zero for every time increment, thereby guaranteeing grid balance. Figure 4-3 shows a bus for oxygen mass flows and a bus for electric power. Flows are represented in this diagram by arrows which always connect one bus to one component.

The depicted model uses four common component types included in Solph. The source class can be used to originate defined inflows to the connected bus. For example, the source “oxygen supply” in the diagram feeds an oxygen mass flow to the oxygen bus, thus simulating an external oxygen source. In contrast to that, a sink object such as the “oxygen demand” component in the diagram is used to define an outflow.

Transformers can have multiple input flows and multiple output flows and are therefore connected to one or more buses. Predefined transformation factors determine how inflows are converted to outflows. Transformers represent plants for energy conversion or production. For instance, the transformer “pressure swing adsorption” is used to model a PSA unit. This plant uses electric power from the electricity bus as input and converts it to an oxygen mass outflow, while the chosen transformation factor represents the specific electricity consumption for oxygen production via PSA.

The last component type depicted in the diagram is the generic storage class. A generic storage is connected to just one bus, but this connection can either be an inflow or an outflow. Depending on the current flow, an intrinsic capacity value of the generic storage is increased or decreased. Therefore, this class can represent some sort of storage. The “oxygen storage” object in the example simulates a storage tank, which can be used to store surplus oxygen from the oxygen bus to feed it back later when there is higher demand. Generic storage components are different from other components in that not only inflows and outflows but also the storage itself is adjustable. Thereby, it is possible to define the capacity of storage options as well as minimum and maximum storage levels in relative shares of the maximum capacity. By selecting these parameters, the usable capacity range of the generic storage can be changed. A minimum storage level of zero and a maximum storage level of one would enable the utilization of the complete capacity range [33].

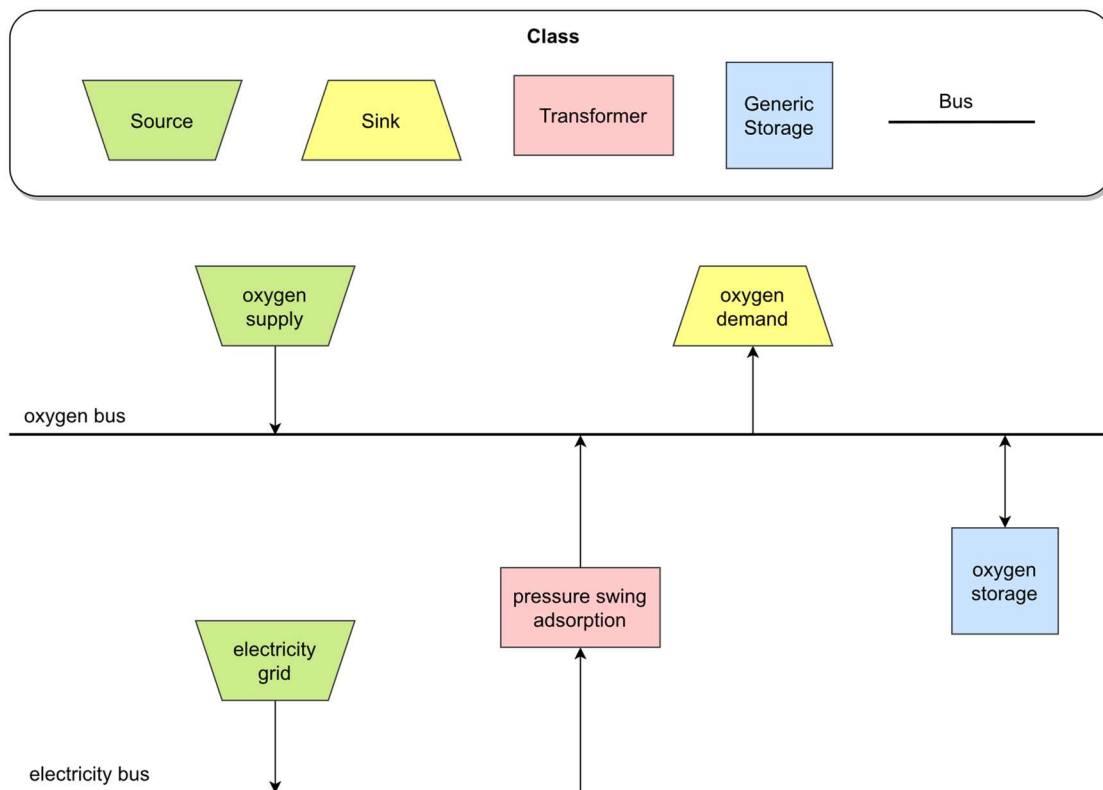


Figure 4-3: Example of an energy system model generated via oemof-solph

In- and outflows of components are specified by giving a nominal value and fixed values. The actual value of the flow for any time increment is then calculated by multiplying the nominal value with the current fixed value. For instance, fixed values can represent load or flow profiles while the nominal value is used to multiply these values. When setting the nominal value to one, fixed values would equal actual values. It is also possible to define minimum and maximum values for flows in relative shares of the nominal value. Analogous to the capacity range of the generic storage, the available load range of a component can thus be limited. Flow definitions can also include a maximum positive gradient and a maximum negative gradient, given in relative share of the nominal value per time increment of the model. It is thus possible to simulate load change limitations. Undefined flow parameters are subject to the optimization of the energy system model [33].

Optimization of a generated energy system model typically aims to minimize costs. Therefore, it is possible to assign variable costs to flows. For example, every kWh of electric energy or every kg of oxygen is then increasing the total cost of the energy system. Furthermore, it is possible to define investment costs for components but also flows. During optimization, these investment costs are multiplied by the maximum capacity or the maximum flow rate of the component or flow. For example, investment costs can be used to optimize the nominal storage capacity of a generic storage or the nominal power of a transformer. Using this option for flows disables the definition of a nominal value, but the definition of fixed values is still

possible. Moreover, a maximum value for the investment flow or the investment component can be defined to limit the possible maximum capacity or maximum flow rate [33]. With the help of other Python libraries, such as “matplotlib” or “pandas”, results from optimization can be stored in Excel files or used for the creation of plots.

4.3 Optimization model

The scenarios introduced in chapter 4.1 represent different combinations of parameters in the Solph energy system model. The energy system model also includes the load and generation profiles of the demand model (see section 3.3) as flow values for corresponding components. Because the profiles from the demand model span four weeks with a resolution of 15 min, the optimization model also uses these values for optimization time and time resolution. The objective of the Solph model is to find optimal operational strategies for all included components while also optimizing the size and capacity of storage tanks and plants by minimizing costs. Figure 4-4 depicts the optimization model with all components and buses. By changing parameters, it is possible to activate or deactivate components to model certain scenarios. Thus, the model can depict and optimize different supply strategies for the steel mill.

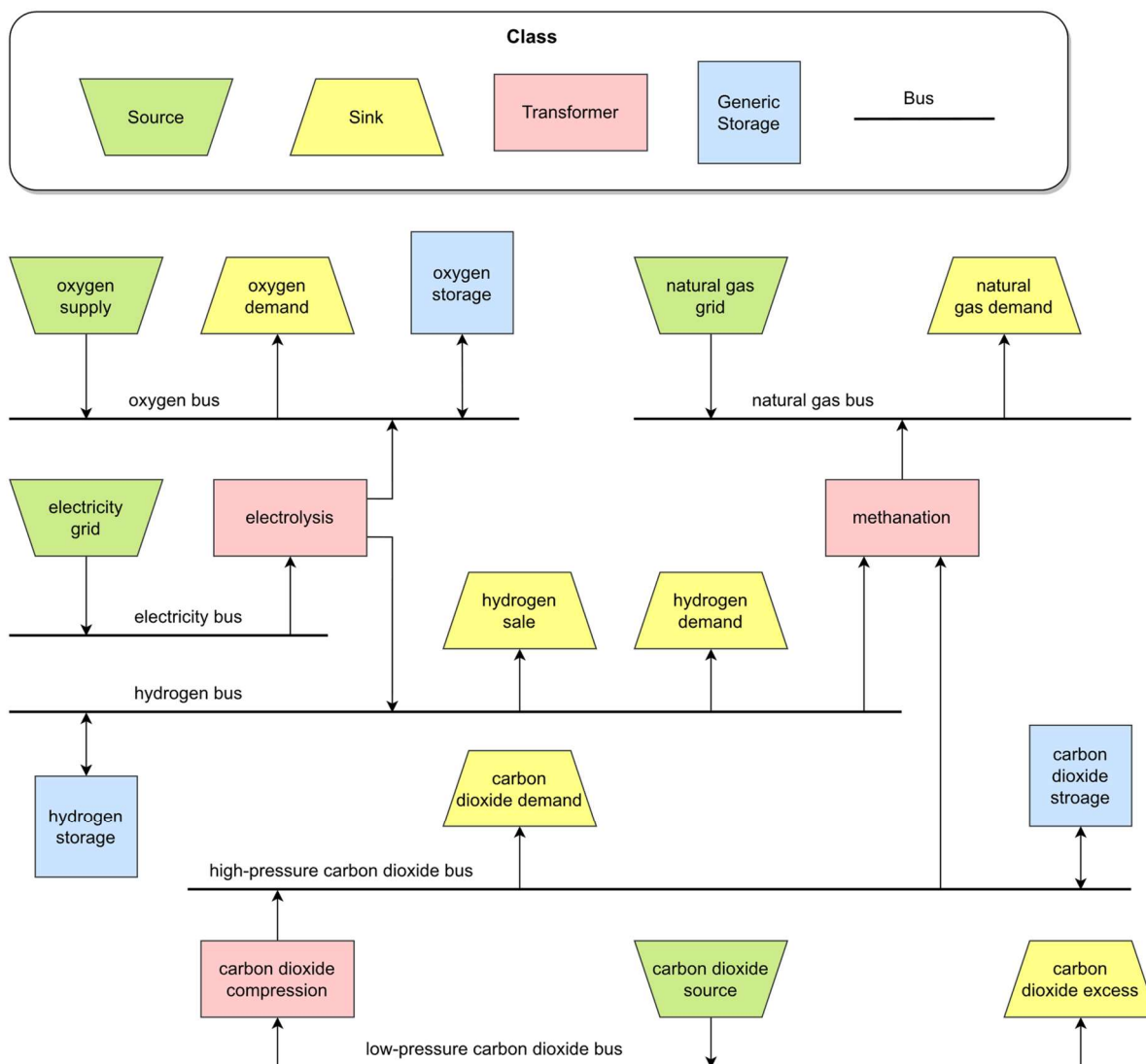


Figure 4-4: Energy system model for optimization

The subsequent paragraphs deal with all buses and components shown in the above flow scheme. Every section illustrates one energy carrier or process gas. The optimization model includes electricity, oxygen, hydrogen and natural gas as well as low- and high-pressure CO₂.

4.3.1 Electric energy

The component “electricity grid” represents the power connection to the public grid. Variable costs for the outflow of the component enable the assignment of electricity prices to the purchased energy. The unit for all electric energy flows is kW_{el}, therefore variable costs in EUR/kWh_{el} are given in the form of time-resolved electricity price profiles (see section 4.4.1).

Energy from the electric grid is then consumed by the electrolysis unit. The electrolyser is not only connected to the electricity but also to the oxygen and hydrogen bus, reflecting the electrolysis process. The capacity of the necessary electrolyser is optimized by changing the electricity inflow to an investment flow and by applying a specific investment cost.

In this model, electric energy is not only supplied to the electrolyser but also to the compressors for hydrogen and CO₂. The methods for implementing and optimizing the compressor electricity demands are described in the following sections for hydrogen supply and CO₂ supply.

4.3.2 Oxygen

Oxygen is either generated by electrolysis or supplied externally by a centralized ASU. The delivery schedule for external supply is managed by an additional code that schedules the deliveries based on the oxygen load profile and a defined delivery time table. Hence, the fulfilment of the demand is guaranteed while inefficient deliveries are avoided. The delivery schedule serves as input for the “oxygen supply” component, while the actual purchased volumes of oxygen are dependent on the demand and additional plant-internal oxygen production via electrolysis. The unit for oxygen flows is kg_{O₂}/h, therefore fixed variable costs in EUR/kg_{O₂} are assigned to the LOX outflow from this component.

The consumption of oxygen in the steel mill is represented by the “oxygen demand” component. The time-resolved oxygen load profile from the demand model is used to define the inflow of this component and thus the oxygen consumption.

For the future scenarios, it is assumed that PEMEL produces oxygen and hydrogen with pressure levels in the range between 10 and 30 bar, similar to the approach of Gorre et al. [5]. Oxygen is then stored in a pressure tank and the mentioned pressure range is used to specify the storage load range. Moreover, it is assumed that these pressure levels are always high enough to supply the oxygen consumers. Therefore, no oxygen compressors are needed. By using the investment mode and an investment cost, the maximum capacity of the oxygen storage tank is subject to optimization.

4.3.3 Hydrogen

The only source of hydrogen is the electrolysis unit. Hydrogen produced via PEMEL is supplied to different components depending on the current scenario. In this energy system model, hydrogen loads are based on the mass flow. Thus, the unit for all hydrogen flows is kg_{H₂}/h.

The sink “hydrogen demand” represents the consumption of the steel mill when hydrogen burners are partially used for ladle heating. This demand is derived from the natural gas load profile. The natural gas demand for affected ladle heaters based on the HHV is converted to the actual thermal power demand based on the LHV of natural gas or hydrogen. Subsequently, this value is used to determine the necessary hydrogen mass flow. On the one hand, deploying hydrogen burners and thereby creating a hydrogen demand decreases the natural gas consumption. On the other hand, the potential for CO₂ generation is decreased if some of the

Oxyfuel burners used for CCU are affected. The resulting hydrogen load profile defines the “hydrogen demand” inflow of the hydrogen bus.

When hydrogen is not utilized in the steel mill but rather sold off to an external consumer, the sink “hydrogen sale” is used. According to Gao and Krishnamurthy [34], typical pressure levels for transporting gaseous hydrogen via tank truck lie in the range between 3 and 7 kpsi or about 207 and 483 bar. Therefore, it is assumed that hydrogen needs to be compressed to a pressure level of 345 bar prior to transport. This compression process is modelled by changing the inflow of the sink to an investment flow. The investment cost represents the cost for the necessary compressor, whereas the electricity costs for compression are calculated by using the electricity price data and the specific energy consumption for compression of hydrogen. These values are used as variable costs for the flow, together with a fixed and negative cost value representing revenue from selling hydrogen.

The third hydrogen consumer in the energy system model is the methanation plant. This component uses inflows from the hydrogen bus and the carbon dioxide bus. The outflow of the transformer is connected to the natural gas bus, thereby representing the production of SNG by the methanation of CO₂. Contrary to the electrolyser, not one of the inflows but rather the outflow is converted to an investment flow in order to optimize the capacity of the methanation plant based on its investment cost.

Analogous to the oxygen bus, the hydrogen bus is connected to a generic storage representing a pressurized gas tank. The storage level of this hydrogen storage depends on the hydrogen pressure level after electrolysis. As with the oxygen storage, the minimum and maximum storage level as well as the investment cost are given as parameters.

4.3.4 Natural gas

In some of the scenarios, natural gas is partially supplied in the form of SNG from the methanation plant. However, the majority of natural gas consumed in the steel mill stems from the public gas grid, represented by the respective source. All natural gas flows are thereby based on the HHV of natural gas. When natural gas is purchased from the gas grid, costs arise from buying the natural gas itself and from buying allowances for resulting CO₂ emissions. Both cost factors are considered by applying fixed prices. The combined natural gas price is then used as a variable cost for the outflow.

To represent the natural gas demand of the steel mill, the “natural gas demand” component is used. The actual inflow values of this sink are defined with the help of the natural gas load profile from the demand model. As mentioned above, if hydrogen is used for ladle heating, the overall natural gas demand decreases.

4.3.5 Carbon dioxide

There exist two different buses for CO₂. The flows from the low-pressure carbon dioxide bus represent the CO₂ exhaust flows after Oxyfuel ladle heating. Via CCU and subsequent compression, the exhaust carbon dioxide bus is connected to the high-pressure carbon dioxide bus. For both buses, all load and generation profiles are based on the mass flow in kg_{CO2}/h.

4.3.5.1 Low-pressure carbon dioxide

CO₂ production for any time increment is given by the CO₂ generation profile obtained from the demand model. This time-resolved profile is implemented by defining the outflow of the “carbon dioxide source”. By converting some of the Oxyfuel burners to hydrogen burners, the exhaust gas available for CCU decreases.

A compressor connects the low-pressure and high-pressure carbon dioxide bus. The mass flow remains unchanged. However, the pressure of the CO₂ is raised, represented by changing the outflow to an investment flow. Analogous to oxygen and hydrogen, it is assumed that pressures in the range between 10 and 30 bar are used for storage as well as for methanation. Investment costs represent the cost for the compressor unit, while the electricity price data and the specific energy consumption for compression of CO₂ are used to calculate the variable electricity costs for operating the compressor.

The amount of CO₂ which can be captured and compressed is limited by the CO₂ demand in the carbon dioxide bus. Unused CO₂ is then exhausted into the atmosphere. The sink component “carbon dioxide excess” represents this exhaustion of surplus CO₂ and thereby guarantees mass balance in the low-pressure carbon dioxide bus. By changing the inflow of the sink to an investment flow with investment costs of zero and a defined maximum investment, the excess mass flow can be limited. Thus, it is possible to completely disable the excess flow and thus force complete compression and subsequent methanation of surplus CO₂.

4.3.5.2 High-pressure carbon dioxide

CO₂ is supplied by the “carbon dioxide compression” component and consumed by the sink “carbon dioxide demand” and the methanation plant. The “carbon dioxide demand” component represents the CO₂ consumption for water treatment. Therefore, the respective CO₂ load profile from the demand model is used to define the actual inflow values of this sink.

Another potential CO₂ consumer or supplier connected to the carbon dioxide bus is the CO₂ storage. Similar to the oxygen storage and hydrogen storage, this component represents a pressurized gas tank. The parameters defining this storage tank are minimum storage level, maximum storage level and investment cost.

4.4 Model for cost calculation

Optimization of the described energy system model aims to minimize costs. Therefore, a cost model is needed to determine these costs. Furthermore, this model serves for the economic assessment of the different scenarios. Formula (4-1) shows how the total annual energy costs (c_{total}) are calculated for each scenario. The annual energy cost (c_{energy}) represents the cost for supplying the demand model with oxygen and direct fuel. c_{inv} contains the annual investment costs for necessary plants, storage tanks and compressors, while the resulting costs from operating those are represented by c_{op} .

$$c_{total} = c_{energy} + c_{inv} + c_{op} \quad (4-1)$$

All costs for this model need to be adjusted to 2020 EUR. This is accomplished by using the cost indices listed in section 9.1. Subsequently, the method for calculating these different costs is described, starting with energy costs and continuing with investment and operational costs.

4.4.1 Energy cost

Equation (4-2) shows how the annual energy cost (c_{energy}) is calculated. c_{O_2} is the annual cost for oxygen, which consists of the purchase cost for LOX and the transportation cost. The LOX cost is calculated by multiplying the specific LOX price, which matches the variable costs for oxygen delivery in the optimization model, with the yearly supplied oxygen mass. To obtain yearly values, the optimization results are simply extrapolated to one year. The transportation cost depends on the cost per delivery and the number of deliveries during one year. In the optimization model, a natural gas price and an emission allowance price are used to define the variable costs for natural gas from the grid. Multiplying the natural gas price by the annual thermal energy supply from the gas grid results in the annual cost for natural gas (c_{NG}). The annual CO₂ mass, which is released when combusting natural gas from the grid, is multiplied by the allowance price to obtain the annual allowance cost (c_{CO_2}). r_{H_2} is the annual revenue from selling hydrogen to an external consumer. The amount of annual sold hydrogen is multiplied by the hydrogen price. Selling hydrogen reduces the total cost for the respective scenario, therefore r_{H_2} is subtracted from the annual energy cost. The annual electricity cost (c_{el}) deserves a more detailed description during the next paragraphs.

$$c_{energy} = c_{el} + c_{O_2} + c_{NG} + c_{CO_2} - r_{H_2} \quad (4-2)$$

It is assumed that the prices for natural gas, allowances and hydrogen are fixed over the whole optimization time. However, for electricity, varying prices are used. Firstly, these prices appear in the optimization model to define variable costs for electricity flows. Secondly, the cost

model uses these prices to calculate the annual electricity cost (c_{el}). Electricity prices for 2020 are obtained by adopting historical spot market prices from the Energy Exchange Austria (EXAA) [35]. Because the load profiles of the demand model span only four weeks, the electricity price profile should also include four weeks with a 15 min resolution. Thus, four connected summer weeks are chosen from the 2020 day-ahead prices. The average day-ahead price for 2020 was 33 EUR/MWh_{el} with a standard deviation of 17 EUR/MWh_{el}, while the four weeks period for the cost model shows an average price of 21 EUR/MWh_{el} with a standard deviation of 14 EUR/MWh_{el}.

E-Control [36] published the average electricity prices for 2020. These prices are used to determine the share of grid charges and taxes on the total electricity price. By multiplying these shares with the average day-ahead price, absolute values for grid charges and taxes are obtained. These values are then added to the spot market prices to give the gross electricity prices. According to the Austrian “Elektrizitätswirtschafts- und -organisationsgesetz (EIWOG) 2010”, plants that produce hydrogen or SNG from renewable electricity sources and have a capacity of more than 1 MWh_{el} are exempt from grid charges [37]. Therefore, the reference scenario uses the gross electricity prices including grid charges and taxes, while the future scenarios only use energy prices plus taxes. In Figure 4-5, the four weeks spanning electricity price profiles used in the optimization model and the original day-ahead energy prices are depicted in form of price duration curves.

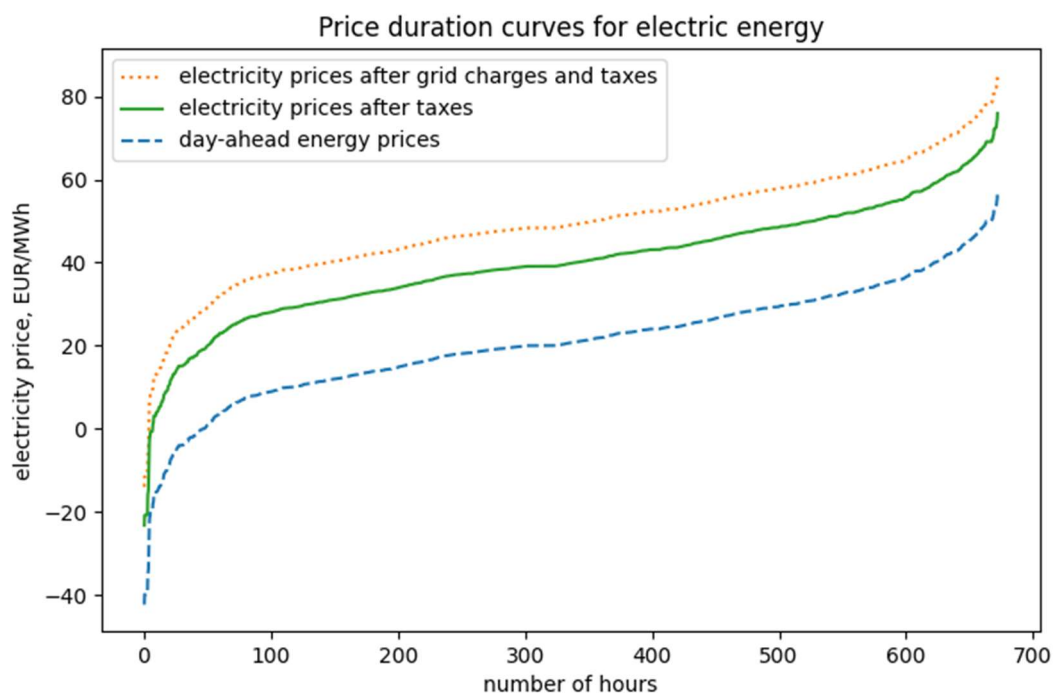


Figure 4-5: Duration curves for varying electricity prices

Potential electricity consumers in the model are the electrolyser and the compressors. To calculate the electricity cost for one 15 min instance of the model, the total electricity consumption during this time is multiplied by the current electricity price. By adding up these cost values for the complete optimization time of four weeks and by extrapolating to a period of one year, the annual electricity cost (c_{el}) is obtained.

4.4.2 Capital and operational expenditures

To calculate the annual investment cost (c_{inv}), equation (4-3) is used to form the equivalent annual costs (EAC) for all necessary investments. Using this equation, the capital expenditure ($CAPEX$) for investment is distributed evenly over the complete lifetime (n) of the asset. Moreover, the EAC also depends on the interest rate (i).

$$EAC = CAPEX * \frac{(1 + i)^n * i}{(1 + i)^n - 1} \quad (4-3)$$

Instead of applying the actual $CAPEX$ of an asset, it is also possible to use the specific $CAPEX$ per unit of asset capacity in equation (4-3). The resulting specific EAC can then be used to define investment costs in the optimization model after adjusting to the optimization time. Multiplication of the specific EAC by the capacity of the asset, for instance by a storage capacity or by an electrolyser capacity, results in the EAC of the investment. The annual investment cost (c_{inv}) is obtained by summing up the EAC values for electrolyser, methanation plant, hydrogen burners, storage tanks and compressors.

Equation (4-4) shows how the annual operational expenditure ($OPEX$) of an asset is calculated, when the $CAPEX$ is known and the relative annual operational expenditure ($OPEX_{\%}$) is given as a percentage of the $CAPEX$.

$$OPEX = CAPEX * OPEX_{\%} \quad (4-4)$$

In this cost model, operational expenditures arise from electrolysis, methanation and gas storage and represent costs for operation and maintenance, excluding electricity costs for electrolysis. Summing up all $OPEX$ -values gives the annual operational cost (c_{op}).

5 MODEL PARAMETERS

The last chapter provided an overview of the optimization model and the cost model. Now, the parameters used for optimizing and cost calculation are described and listed. Firstly, the technical parameters for the optimization model components are depicted. The second part of this chapter illustrates the economic parameters used for variable costs and investment costs in the optimization model as well as for cost calculation in the cost model.

5.1 Technical parameters

Table 5-1 shows technical parameters for electrolyser, methanation plant and storage tanks. In chapter 3.5.2, typical efficiencies for PEMEL systems are listed. After assessing these cited values, a PEMEL system efficiency of 65 %_{HHV} is chosen for the optimization model. The specific energy demands for hydrogen and oxygen production are then calculated from this efficiency. For methanation, parameters are obtained from chapter 3.5.3.

As described in chapter 4.3, it is assumed that the storage level of gas tanks is varied by changing the PEMEL output pressure for hydrogen and oxygen or by changing the output pressure of the CO₂ compressor. Storage pressures range between 10 bar and 30 bar, corresponding to 1 MPa and 3 MPa. Gorre et al. [5] used a maximum storage capacity of 3 000 kg_{H₂} for their hydrogen storage model. Thus, a maximum storage capacity of about 33 800 m_s³ is used as investment maximum for gaseous hydrogen storage, oxygen storage and CO₂ storage.

Table 5-1: Technical parameters for production units and storage

Parameter	Unit	Value	Reference
<i>PEMEL</i>			
efficiency	kWh _{H₂} , HHV/kWh _{el}	0.65	[20, 24, 27]
specific energy demand H ₂	kWh _{el} /kg _{H₂}	61	own calculation
specific energy demand O ₂	kWh _{el} /kg _{O₂}	7.6	own calculation
load range	% _{nom}	0-100	[24]
<i>methanation</i>			
efficiency	kWh _{CH₄} , HHV/kWh _{H₂} , HHV	0.62	calculated from [30]
load range	% _{nom}	70-100	[31]
load gradient	% _{nom} /min	3	[5]
<i>gas storage</i>			
pressure range	MPa	1-3	[5]
load range	% _{nom}	33-100	[5]
maximum capacity	m _s ³	33 800	[5]
<i>liquid storage</i>			
load range	% _{nom}	10-100	own assumption
maximum capacity	kg _{O₂}	38 400	own assumption (see section 5.2)

The technical model parameters for CO₂ and hydrogen compression are listed in Table 5-2. Equation (5-1) is used to calculate the specific adiabatic enthalpy (h_{ad}) for the compression of different gases in kJ/kg. R' is the specific gas constant of the considered gas in kJ/(kg K) and κ is the heat capacity ratio of the gas. T_1 and p_1 represent respectively the inlet temperature in K and the inlet pressure in Pa, while p_2 is the outlet pressure in Pa.

$$h_{ad} = R' T_1 \left(\frac{\kappa}{\kappa - 1} \right) \left[\left(\frac{p_2}{p_1} \right)^{(\kappa-1)/\kappa} - 1 \right] \quad (5-1)$$

Model parameters

To represent a more realistic compression, the specific adiabatic enthalpy (h_{ad}) is then converted to the specific polytropic enthalpy (h_{poly}) by using equation (5-2). In this formula, η_{ad} is the adiabatic efficiency of the compressor.

$$h_{poly} = h_{ad}/\eta_{ad} \quad (5-2)$$

Peters et al. [38] listed typical values for η_{ad} depending on the compressor type. The compressors in the energy system model are assumed to be motor-driven and reciprocating with an adiabatic efficiency of 0.7. Furthermore, it is assumed that the inlet temperature is always 20 °C or 293.15 K. The optimization model can only handle linear equations, thus mean pressures are used to deal with altering inlet and outlet pressure levels. For the low-pressure CO₂ in the exhaust flow, a pressure of 1 bar or 0.1 MPa is assumed. CO₂ is then compressed to the storage or methanation level of 1-3 MPa. Thus, a mean pressure of 2 MPa is used for p_2 . Similarly, the hydrogen compressor is supplied from the electrolysis and storage pressure level with 1-3 MPa, resulting in a mean pressure of 2 MPa for the inlet. Using these temperature and pressure values as well as R' and κ respectively for CO₂ and hydrogen, it is possible to calculate the specific adiabatic enthalpy (h_{ad}) and subsequently the specific polytropic enthalpy (h_{poly}) for compression. In the table below, the latter value is listed as specific energy demand.

Table 5-2: Technical parameters for compressors

Parameter	Unit	Value	Reference
<i>CO₂ compression</i>			
mean inlet pressure	MPa	0.1	own assumption
mean outlet pressure	MPa	2	own assumption
specific energy demand	kWh _{el} /kg _{CO2}	0.094	own calculation
<i>H₂ compression</i>			
mean inlet pressure	MPa	2	own assumption
mean outlet pressure	MPa	35	own assumption
specific energy demand	kWh _{el} /kg _{H2}	2.142	own calculation

5.2 Capital and operational expenditures

Table 5-3 lists specific investment costs, relative annual operational expenditures and lifetimes for electrolyser, methanation unit, storage tanks and hydrogen burner. For the electrolyser, a specific CAPEX exists for small-scale and large-scale applications. The small-scale value is used in scenarios PEMEL 1 and SNG 1, where electrolysis is supplying only a hydrogen demand. In scenarios PEMEL 2 and SNG 2, electrolysers with much higher capacities are needed to supply the oxygen demand of the steel mill. Therefore, the large-scale specific CAPEX is applied in these scenarios. The small-scale specific CAPEX of 2 000 EUR/kW_{el} is chosen by assessing PEMEL investment costs cited in chapter 3.5.2.2. According to Nguyen et al. [27], specific investment costs for electrolysers highly depend on the installed capacity. Assuming a PEMEL capacity in the range of 10 MW_{el} for complete oxygen provision, a large-scale specific CAPEX of 1 000 EUR/kW_{el} is chosen.

Gorre et al. [5] used 490 EUR/kg_{H₂} as specific CAPEX for hydrogen storage, translating to about 43.5 EUR/m_s³. In comparison, van Leeuwen and Mulder [7] used 60 EUR/m_s³. Therefore, a unit-CAPEX of 50 EUR/m_s³ is applied for the hydrogen storage tank in this thesis. Analogous to the maximum storage capacity, this value is then also used for oxygen storage and CO₂ storage.

In their work, Hanak et al. [39] evaluated the techno-economic performance of cryogenic oxygen storage. To calculate specific investment costs, they used a cryogenic storage tank described by Hu et al. [40] as reference. For this storage tank, Hu et al. assumed a capacity of 2 500 m³ and, adjusted to 2020 EUR by using the cost indices from section 9.1, an equipment cost of about 0.74 million EUR.

According to Peters et al. [38], specific equipment costs can be obtained from such reference values by applying the so-called “six-tenths factor rule” shown in equation (5-3). Using the purchase cost for a reference plant b ($cost_b$) and the capacity of plant b ($capacity_b$) as well as the capacity for plant a ($capacity_a$), the purchase cost for plant a ($cost_a$) can be calculated. As a rule of thumb, the cost capacity exponent (z) can be set to 0.6 when there is not enough information for a more accurate assumption.

$$cost_a = (cost_b) \left(\frac{capacity_a}{capacity_b} \right)^z \quad (5-3)$$

It is thus possible to estimate investment costs for cryogenic oxygen storage depending on the storage capacity. Figure 5-1 shows the resulting function for the storage investment cost over the storage capacity in kg_{O₂}. Storage capacities are calculated by using the density of liquid oxygen with 1 280 kg_{O₂}/m³ [39].

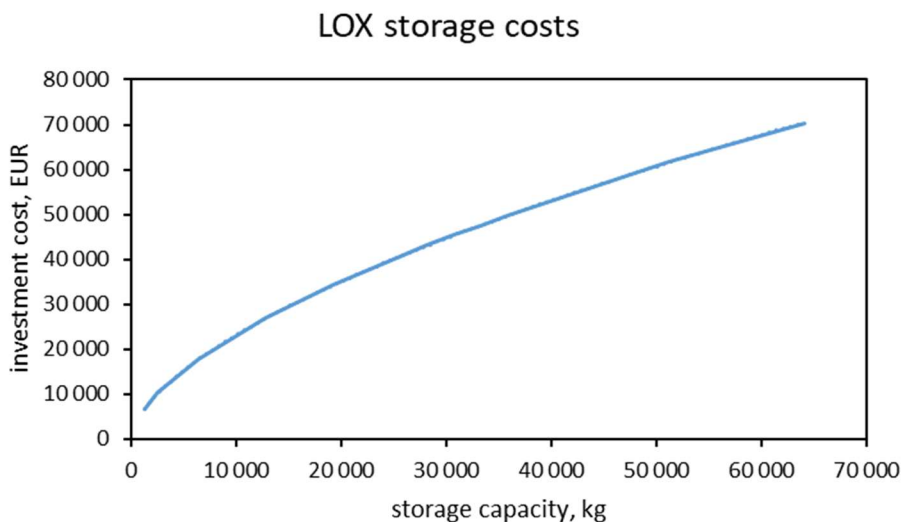


Figure 5-1: Investment costs for cryogenic storage tanks

However, this cost function is non-linear and the optimization model can only solve linear equations. It is therefore necessary to piecewise linearize the storage cost function. After some sample optimizations, it was estimated that the capacity of the cryogenic oxygen storage is in the range between 20 and 30 m³, translating to 25 600 and 38 400 kg_{O2}. Using the cost function, some sample points within the mentioned capacity range were calculated and plotted in Figure 5-2. The dashed line in this plot represents the linear regression, of which the coefficients are also shown in the plot. The resulting investment costs for cryogenic storage consist of a specific CAPEX, corresponding to the slope of the line, and the y-intercept, which is referred to as fixed CAPEX.

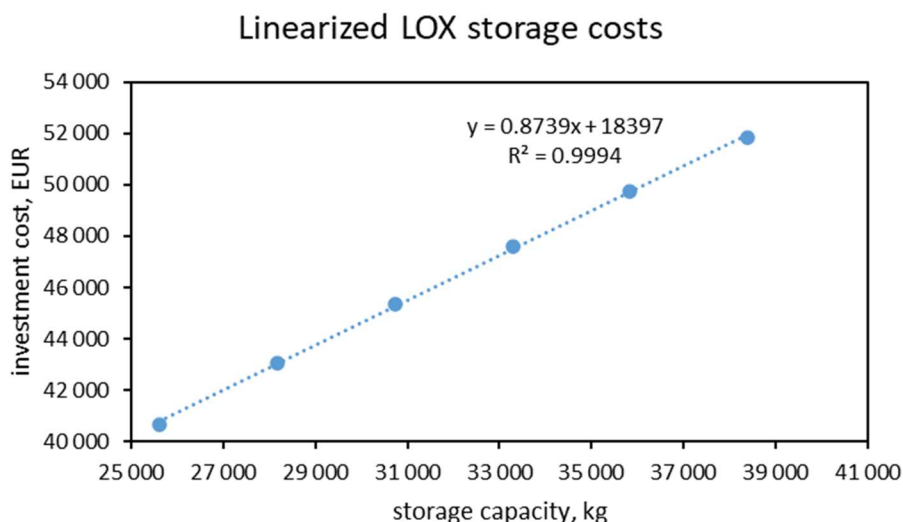


Figure 5-2: Linearized investment costs for cryogenic storage tanks

Model parameters

By using information from our project partners concerning burner investment costs, the total CAPEX for one hydrogen burner is estimated to value 80 000 EUR. In the cost model, this parameter is then simply multiplied by the number of hydrogen burners.

Table 5-3: Economic parameters for production units, storage and hydrogen burners

Parameter	Unit	Value	Reference
<i>PEMEL</i>			
specific CAPEX (small-scale)	EUR/kW _{el}	2 000	[8, 24]
specific CAPEX (large-scale)	EUR/kW _{el}	1 000	[27]
OPEX%	% _{CAPEX}	2.75	[5]
lifetime	a	20	[5]
<i>methanation</i>			
specific CAPEX	EUR/kW _{CH₄, HHV}	450	[5]
OPEX%	% _{CAPEX}	3	[5]
lifetime	a	20	[5]
<i>gas storage</i>			
specific CAPEX	EUR/m _s ³	50	[5, 7]
OPEX%	% _{CAPEX}	1	[5]
lifetime	a	20	[5]
<i>liquid storage</i>			
specific CAPEX	EUR/kg _{O₂}	0.87	calculated from [39, 40]
fixed CAPEX	EUR	18 400	calculated from [39, 40]
OPEX%	% _{CAPEX}	1	[5]
lifetime	a	20	[5]
<i>hydrogen burner</i>			
CAPEX	EUR/burner unit	80 000	project partners
lifetime	a	20	own assumption

Model parameters

In their book, Peters et al. [38] estimated purchase costs of different compressor types depending on the installed capacity in kW_{el} by applying a modified version of the “six-tenths factor rule”. Instead of 0.6, they used a cost capacity exponent of about 0.9 for a reciprocating and motor-driven compressor. Typical compressor capacity ranges for the optimization model were estimated to lie between 200 and 500 kW_{el} for hydrogen compression and between 1 and 40 kW_{el} for CO₂ compression. Thus, it is possible to piecewise linearize the cost function for the compressors. The resulting specific CAPEXs and the fixed CAPEXs are listed in Table 5-4.

Table 5-4: Economic parameters for compressors

Parameter	Unit	Value	Reference
<i>CO₂ compression</i>			
specific CAPEX	EUR/kW _{el}	1 390	calculated from [38]
fixed CAPEX	EUR	1 750	calculated from [38]
lifetime	a	10	own assumption
<i>H₂ compression</i>			
specific CAPEX	EUR/kW _{el}	1 030	calculated from [38]
fixed CAPEX	EUR	35 800	calculated from [38]
lifetime	a	10	own assumption

5.3 Energy costs

The following section deals with prices used in the optimization and cost model and with the specified framework conditions. These model parameters are also shown in Table 5-5. As described in chapter 4.4.1, varying prices based on historic spot market data from 2020 are used for electricity. By adding absolute values for only taxes or grid charges and taxes, the electricity costs for the future scenarios (mean price after taxes) or the reference scenario (mean price after grid charges and taxes) are calculated.

The average natural gas price for 2020, including the energy price, grid charges and taxes, is provided by E-Control [41]. In their market auction report, the European Energy Exchange AG (EEX) [42] published CO₂-emission allowance prices for 2020. A fixed allowance price is then obtained by calculating the average price for the complete year. Šulc and Ditl [43] cite LOX prices for the Czech Republic and Germany. Moreover, they give prices for the delivery of LOX, assuming a transport distance of 150 km. In this thesis, the more expensive LOX price and transport cost for Germany are used as model parameters.

Model parameters

A hydrogen selling price of 3.5 EUR/kg_{H2} is chosen as model parameter. Thus, the assumed price is lower than typical production costs for green hydrogen (see chapter 3.5.2.4).

Table 5-5: Prices and framework conditions

Parameter	Unit	Value	Reference
<i>electricity prices</i>			
mean energy price	EUR/MWh _{el}	21	[35]
mean price after taxes	EUR/MWh _{el}	40	calculated from [36]
mean price after grid charges and taxes	EUR/MWh _{el}	49	calculated from [36]
standard deviation	EUR/MWh _{el}	14	[35]
<i>fixed prices</i>			
natural gas energy price	EUR/MWh _{NG, HHV}	15.17	[41]
grid charges for natural gas	EUR/MWh _{NG, HHV}	2.56	[41]
taxes for natural gas	EUR/MWh _{NG, HHV}	10.27	[41]
gross natural gas price	EUR/MWh _{NG, HHV}	28.00	[41]
allowance price	EUR/t _{CO2}	24.5	[42]
LOX price	EUR/t _{O2}	105	[43]
LOX transport cost	EUR/delivery	50	[43]
H ₂ selling price	EUR/kg _{H2}	3.5	[21, 23, 28]
<i>framework conditions</i>			
interest rate	%	4	[44]

6 RESULTS

By using the parameters presented in the previous chapter, optimization runs are carried out for the reference scenario and the four future scenarios. Following, results from the optimizations and cost calculations are presented and assessed. Thereby, this chapter aims to answer the research questions of this thesis.

6.1 Optimized supply strategies

Optimization of the oemof models determines the optimal plant layouts and the optimal operational strategies for supplying the demand model while minimizing costs and satisfying all scenario restrictions. The optimized plant layouts proposed for the different scenarios are represented via selected key indicators. These plant layout indicators are listed in Table 6-1 and include nominal capacities for implemented production plants and storage units as well as annual production volumes for hydrogen and SNG.

A clear difference can be seen when comparing the hydrogen demand-driven scenarios PEMEL 1 and SNG 1 with the oxygen demand-driven scenarios PEMEL 2 and SNG 2. This is because the oxygen demand of the steel mill is much greater than possible hydrogen demands from ladle heating or methanation. Therefore, electrolyzers that only focus on supplying hydrogen can be much smaller. On the other hand, electrolysis has to cover the oxygen demand of the steel mill all alone in scenarios PEMEL 2 and SNG 2. Electrolyser capacities thus need to be significantly higher in these cases.

Regular LOX deliveries are a necessity in scenarios PEMEL 1 and SNG 1. Storage capacities for oxygen thus need to be higher compared to scenarios without LOX delivery. CO₂ storage is needed in all scenarios to balance CO₂ generation from CCU and CO₂ demand for water treatment. However, even greater storage capacities are needed for scenarios PEMEL 1, SNG 1 and SNG 2. This is because additional CO₂ demands arise from methanation in the SNG scenarios while operating hydrogen burners instead of natural gas burners decreases the CO₂ availability in scenario PEMEL 1. The maximum storage capacity in scenario SNG 1 is thereby much higher than in scenario SNG 2. A possible explanation for this is that hydrogen production is less flexible and thus less CO₂ availability-actuated in scenario SNG 1.

Table 6-1: Indicators for optimized plant layouts

Plant layout indicator	Unit	PEMEL 1	PEMEL 2	SNG 1	SNG 2
<i>PEMEL</i>					
nominal capacity	kW _{el}	2 440	11 100	2 450	10 600
H ₂ production	t/a	310	1 040	334	1 040
<i>methanation</i>					
nominal capacity	kW _{CH₄, HHV}	-	-	996	1 070
SNG production	MWh _{CH₄, HHV/a}	-	-	8 290	8 290
<i>storage tanks</i>					
O ₂ storage capacity	kg _{O₂}	38 800	22 000	35 800	23 100
CO ₂ storage capacity	kg _{CO₂}	2 250	281	6 430	2 700
H ₂ storage capacity	kg _{H₂}	848	-	-	-

Following, the optimized operational strategies in the future scenarios are presented. Plots are used to visualize oxygen mass flows, thermal power, hydrogen mass flows and CO₂ mass flows in the optimized energy system model for every scenario. The flow values are normalized using the respective maximum demand. Demand flows such as steel mill loads or demands from production plants are plotted in the negative direction of the y-axis. The figures show then how these demands are supplied using on-site production or storage outflows. These supply flows are represented by positive values. Simultaneous flows, both negative or positive ones, are added up to give the current total demand flow or total supply flow. All plots show representatively only the first week of the optimization time.

Results

Starting with scenario PEMEL 1 and Figure 6-1, it can be seen that most of the oxygen demand is covered by the storage tank, while only a comparatively small fraction is supplied by the electrolyser. This is because oxygen is mostly provided in form of LOX purchases. After delivery, LOX is vaporized and stored for future utilization in the steel mill. In this scenario, the electrolyser operation focuses on supplying hydrogen burners for ladle heating. The resulting hydrogen load profile is shown in the subplot “hydrogen supply”. Providing thermal energy by combusting hydrogen would result in a decreased natural gas demand. In the respective subplot “natural gas supply”, the natural gas demand is unchanged from the original load profile. However, energy provision by hydrogen is represented as a supply flow, thus reducing the natural gas need from the gas grid.

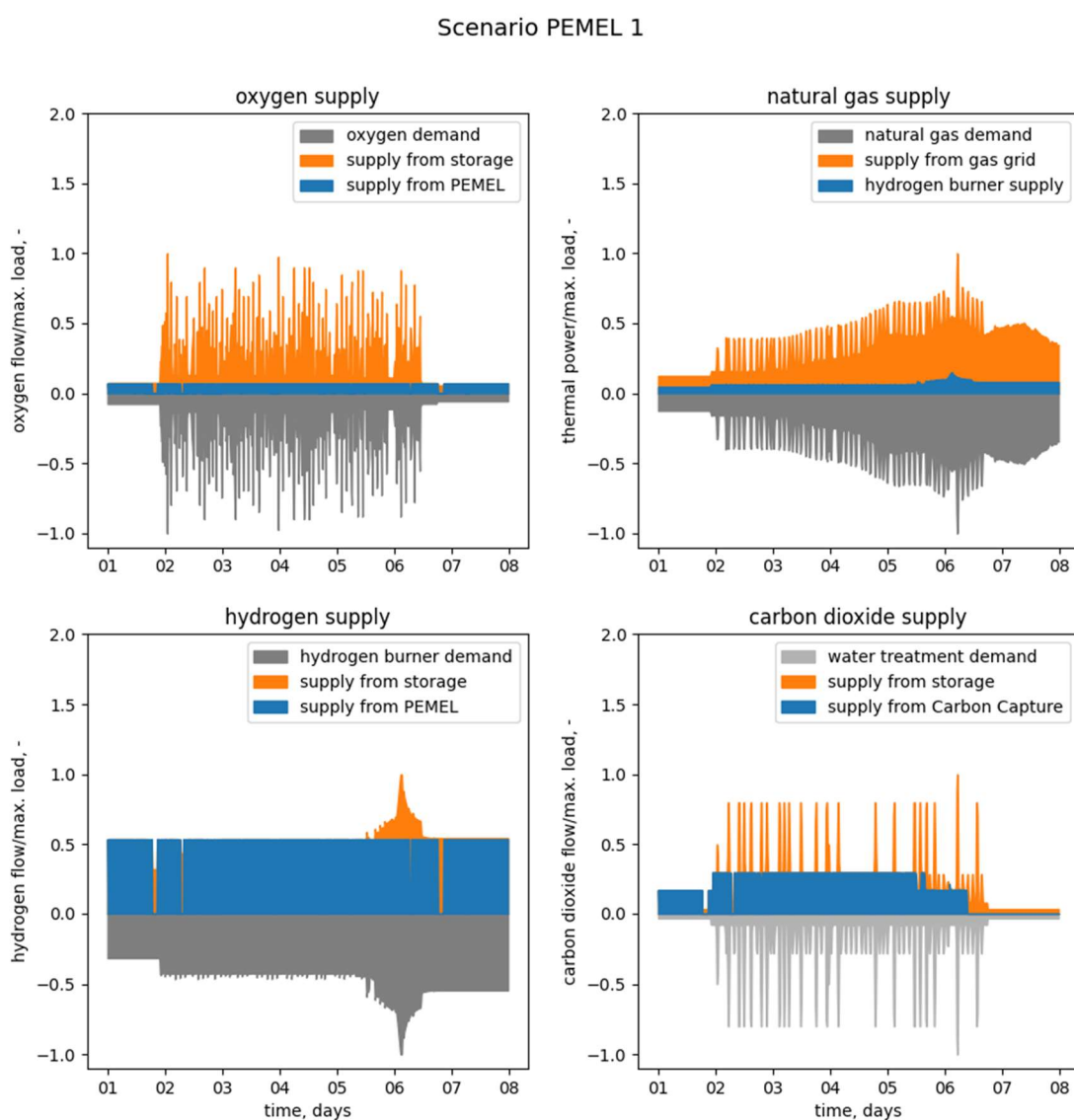


Figure 6-1: Supply strategies for scenario PEMEL 1

Results

Figure 6-2 depicts demand flows and supply flows for scenario PEMEL 2. Contrary to the situation in the previous scenario, electrolysis produces now enough oxygen to supply the steel mill without additional LOX deliveries. Oxygen storage is therefore only used to balance PEMEL production and steel mill demand. As shown in the figure, hydrogen produced from electrolysis is completely sold off. Because in this scenario hydrogen is not used to substitute natural gas in any way, the natural gas demand is only covered by supply from the gas grid.

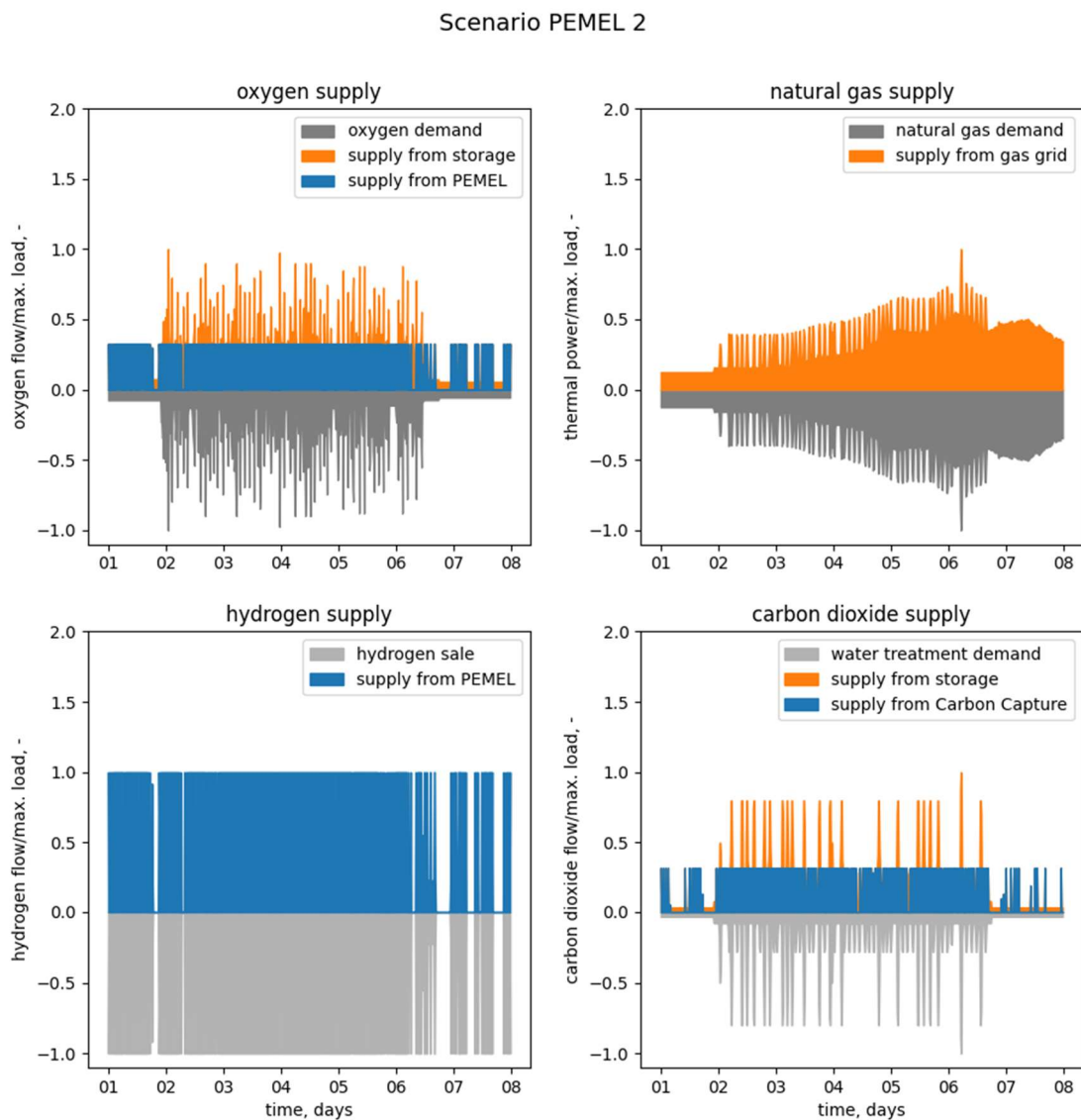


Figure 6-2: Supply strategies for scenario PEMEL 2

Results

Analogous to scenario PEMEL 1, electrolysis focuses on covering a predefined hydrogen demand in scenario SNG 1. Accordingly, LOX deliveries are necessary to compensate for decreased oxygen production rates. The resulting oxygen and hydrogen flows are presented in Figure 6-3. Hydrogen is utilized in a subsequent methanation process, where SNG is produced from hydrogen and CO₂. As depicted in the subplot “natural gas supply”, SNG is used to supply the steel mill with thermal energy, thereby slightly reducing the natural gas need from the gas grid. Regarding the “carbon dioxide supply” subplot, the potential for CO₂ generation from CCU is completely exploited. Surplus CO₂, which is not needed for water treatment, is then fully utilized in the methanation plant.

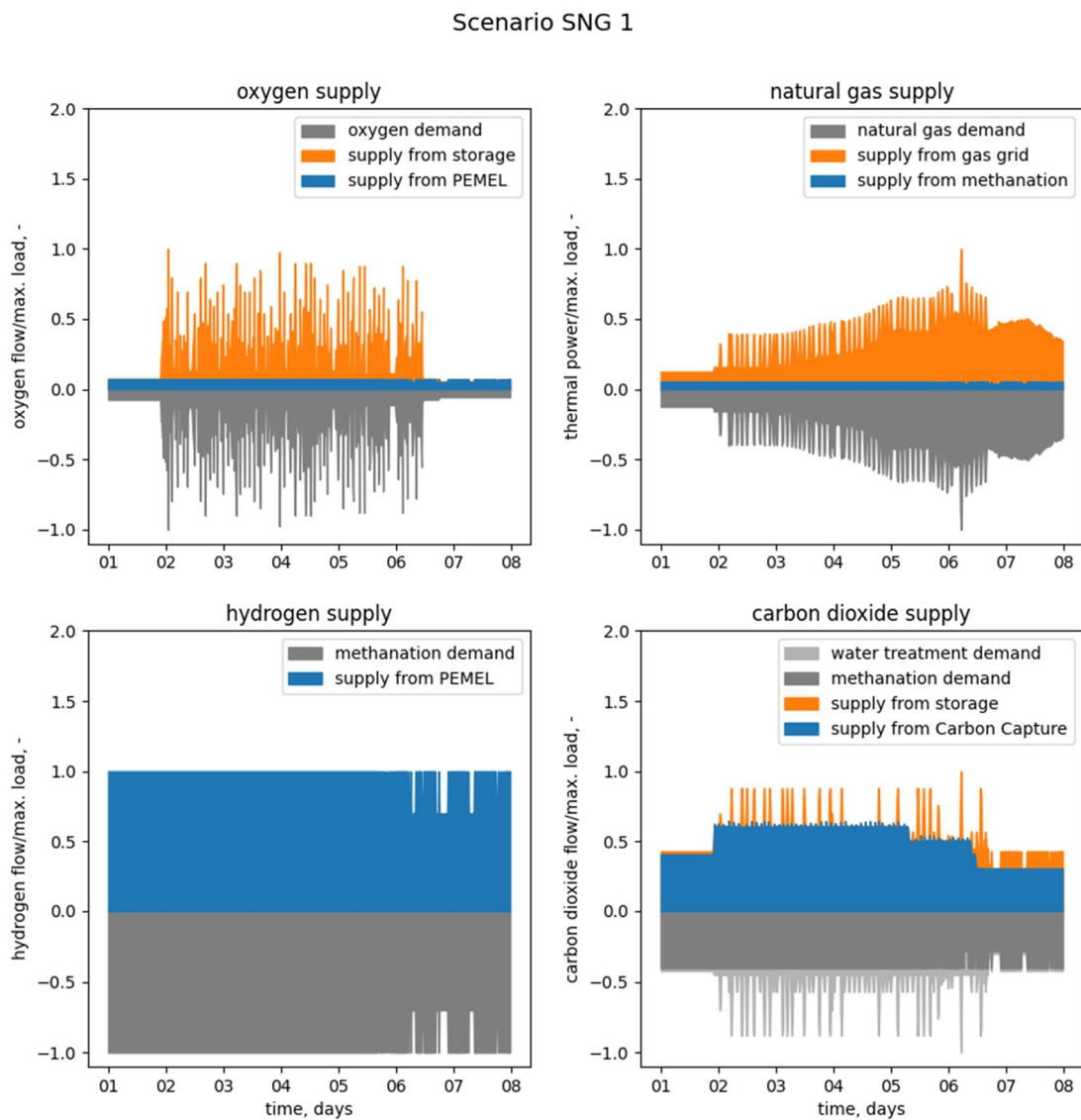


Figure 6-3: Supply strategies for scenario SNG 1

As illustrated in Figure 6-4, oxygen for the steel mill is only provided via the electrolyser in scenario SNG 2. The majority of thereby generated hydrogen is sold off, but a part of it is utilized for the production of SNG via methanation. The “natural gas supply” subplot depicts how SNG is then utilized in the steel mill to substitute natural gas from the gas grid. A part of the CCU potential is utilized for water treatment, while the remaining potential is used to provide the feedstock for methanation.

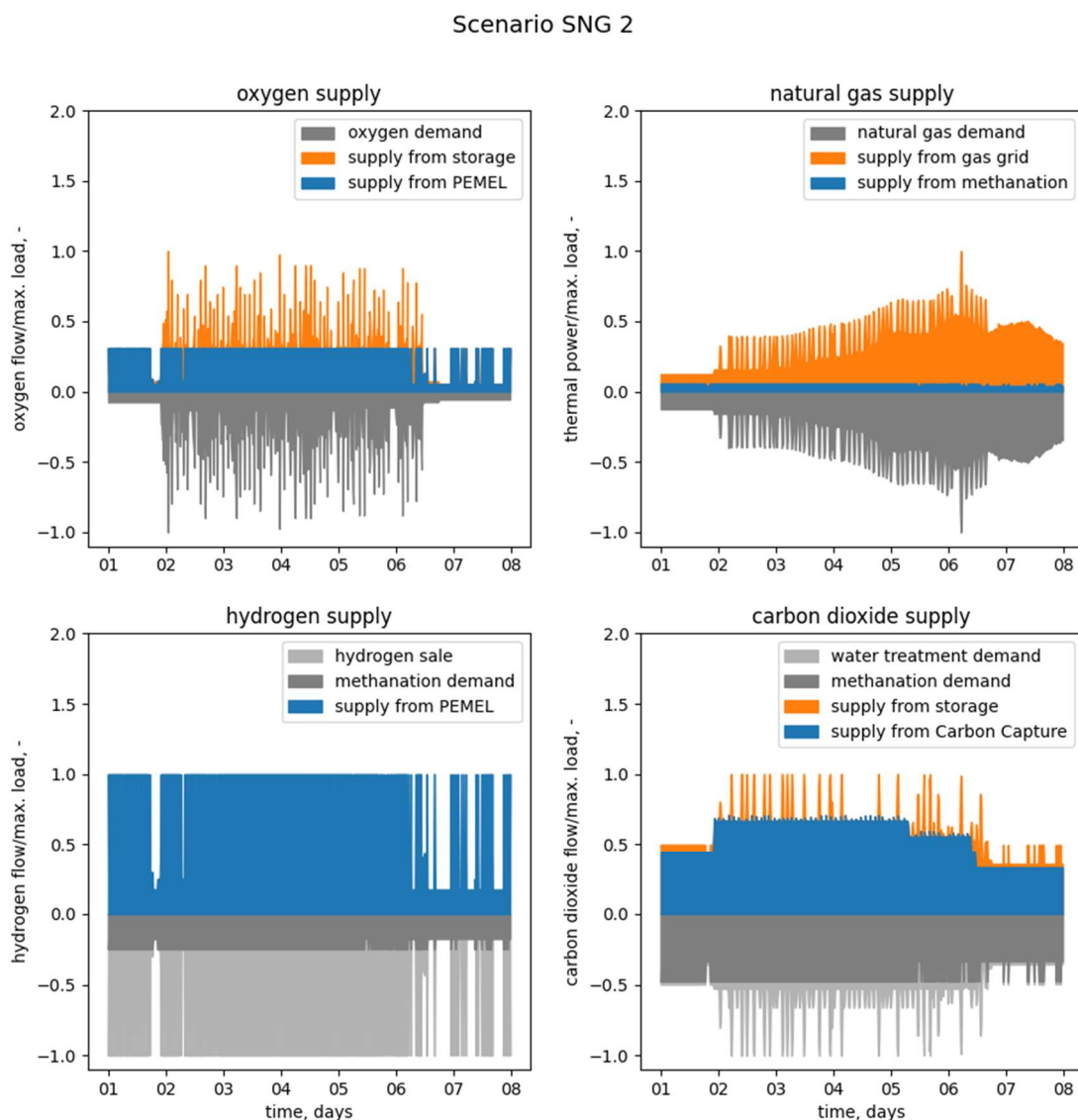


Figure 6-4: Supply strategies for scenario SNG 2

According to the aim of this thesis, PEMEL should not only cover the oxygen and thermal energy demands of the steel mill in a time-actuated manner. Rather, electrolysis should be used to provide a flexibility option for better integration of intermittent energies into the electricity grid. A potential indicator for surplus electricity in the grid due to intermittent energy sources is the current electricity price. Therefore, cost optimization should also aim to integrate such energy sources more efficiently. Representatively, Figure 6-5 depicts the

electricity price for PEMEL operation and the power consumption for electrolysis in scenario PEMEL 2 over one week. Looking at this figure, a connection between electricity price and PEMEL operation can be seen. Electrolysis is avoided when electricity prices are high, while low prices lead to maximum power consumption. Figures illustrating the electricity utilization in the other future scenarios can be found in section 9.2.

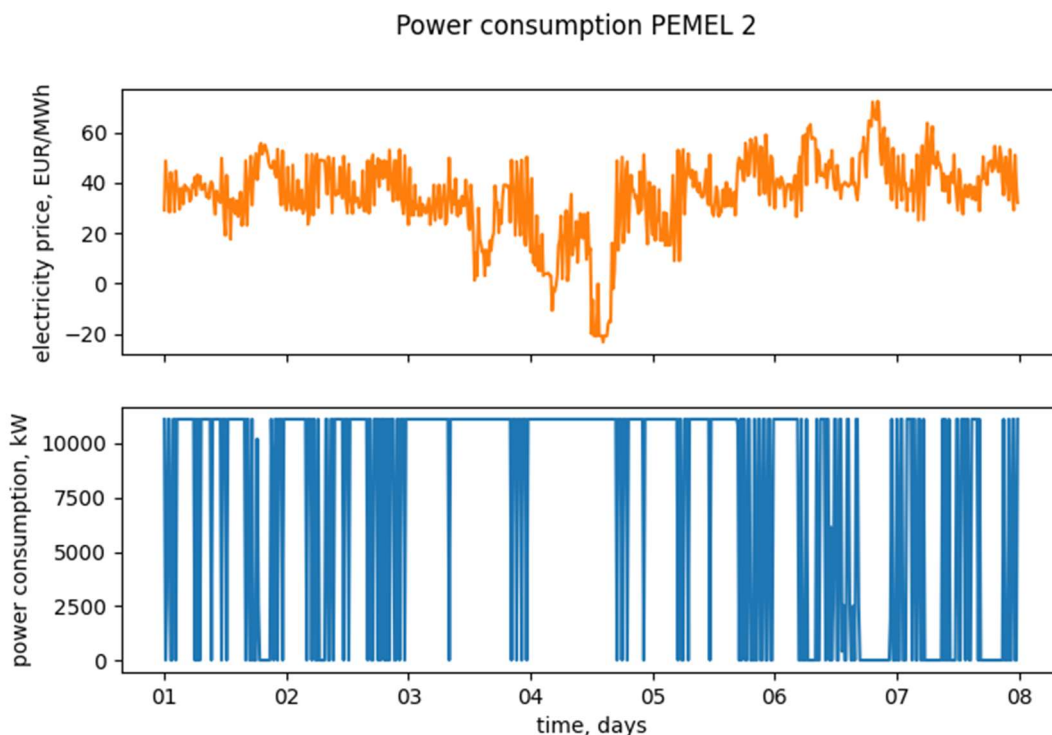


Figure 6-5: Electricity utilization in scenario PEMEL 2

Full load hours provide another way to indicate the flexibility and therefore the demand side management potential. Less flexibility leads to higher full load hours, while a more flexible operation strategy results in more frequent load changes, longer downtimes and thus lower full load hours. Table 6-2 shows the annual PEMEL full load hours for all future scenarios. Moreover, these full load hours are divided by the number of hours in one year, amounting to 8 760 h/a, to calculate the annual load factor of the electrolyser. Again, lower values indicate more flexibility.

The suitability of the scenarios for demand side management is also shown by the mean purchased electricity price ($p_{el,PEMEL}$) which is calculated based on equation (6-1). The annual electricity cost for operating the electrolyser ($c_{el,PEMEL}$) is divided by the annual amount of electric energy consumed by the electrolyser ($W_{el,PEMEL}$). The mean purchased electricity price can then be compared to the actual mean electricity price (mean price after taxes, see Table 5-5). For an electrolyser with a load factor of 100 %, these two values would be identical. Thus, lower mean purchased electricity prices indicate a higher demand side flexibility.

$$p_{el,PEMEL} = \frac{C_{el,PEMEL}}{W_{el,PEMEL}} \quad (6-1)$$

Other indicators listed in Table 6-2 are the annual sold off hydrogen mass and CO₂ emission savings. For the indicator “CO₂ savings from H₂ sales”, it is assumed that producing and selling green hydrogen via PEMEL leads to an appropriate demand reduction for grey hydrogen. Further, it is assumed that PEMEL is only utilizing electricity from zero CO₂ emission energy sources thanks to flexible and electricity price-actuated operation. According to Muradov [45], about 7.8 kg_{CO2}/kg_{H2} are emitted when hydrogen is produced via SR. Using this value, the annual CO₂ savings from hydrogen selling are calculated. To determine the other two emission saving indicators, the amount of natural gas directly substituted via hydrogen or SNG is assessed. Then, the annual CO₂ savings are calculated under the simplifying assumption that natural gas contains only CH₄. Adding up all values for emission savings gives the total CO₂ savings for each scenario.

Table 6-2: Key performance indicators for optimized supply strategies

KPI	Unit	PEMEL 1	PEMEL 2	SNG 1	SNG 2
PEMEL full load hours	h/a	7 770	5 680	8 320	5 960
PEMEL annual load factor	%	88.7	64.8	95.0	68.0
actual mean electricity price	EUR/MWh _{el}	40	40	40	40
mean purchased electricity price	EUR/MWh _{el}	38	33	39	35
sold off H ₂	t _{H2} /a	-	1 040	-	701
CO ₂ savings from H ₂ sales	t _{CO2} /a	-	8 080	-	5 480
CO ₂ savings from H ₂ utilization	t _{CO2} /a	2 050	-	-	-
CO ₂ savings from SNG utilization	t _{CO2} /a	-	-	1 480	1 480
total CO ₂ savings	t _{CO2} /a	2 050	8 080	1 480	6 960

6.2 Economic assessment

This chapter deals with the question if the future scenarios are not only ecologically but also economically beneficial. The economic performance of the different scenarios is indicated by the annual costs explained in chapter 4.4. Table 6-3 lists these costs for the future scenarios as well as for the reference scenario. To assess how economically viable a scenario is, its total annual energy costs need to be compared to the reference scenarios costs. Scenarios PEMEL 1 and SNG 1 are more expensive than the reference scenario. Therefore, these scenarios are

not economically viable under the given framework conditions. Meanwhile, the total annual energy costs for scenarios PEMEL 2 and SNG 2 are lower than for the reference scenario due to high revenues from selling hydrogen.

Table 6-3: Annual costs for reference case and future scenarios

Cost component	Unit	Reference	PEMEL 1	PEMEL 2	SNG 1	SNG 2
annual electricity cost	EUR	1 910	713 000	2 170 000	806 000	2 240 000
annual oxygen cost	EUR	893 000	632 000	0	612 000	0
annual natural gas cost	EUR	1 770 000	1 450 000	1 770 000	1 540 000	1 540 000
annual allowance cost	EUR	306 000	251 000	306 000	266 000	266 000
annual hydrogen revenue	EUR	0	0	-3 630 000	0	-2 460 000
annual energy cost	EUR	2 970 000	3 050 000	628 000	3 220 000	1 590 000
annual investment cost	EUR	5 170	546 000	931 000	503 000	929 000
annual operational cost	EUR	447	153 000	314 000	162 000	314 000
total annual energy cost	EUR	2 980 000	3 750 000	1 870 000	3 890 000	2 830 000

Figure 6-6 shows how different cost components contribute to the overall cost for each future scenario. Cost values are divided by the total cost of the respective scenario, excluding hydrogen revenues, to give relative cost shares. Therefore, the red cost-share bars for all cost components always add up to 100 %, while the green bars show the ratio between hydrogen revenue and total cost. Cost structures look quite similar for the hydrogen demand-driven scenarios PEMEL 1 and SNG 1 and the oxygen demand-driven scenarios PEMEL 2 and SNG 2 respectively. For hydrogen demand-actuated scenarios, natural gas costs are predominant, while electricity costs take over in scenarios PEMEL 2 and SNG 2. Generally, costs are much higher for oxygen demand-actuated scenarios due to higher electricity and investment costs, but the resulting total costs are then massively reduced when regarding revenues from hydrogen selling.

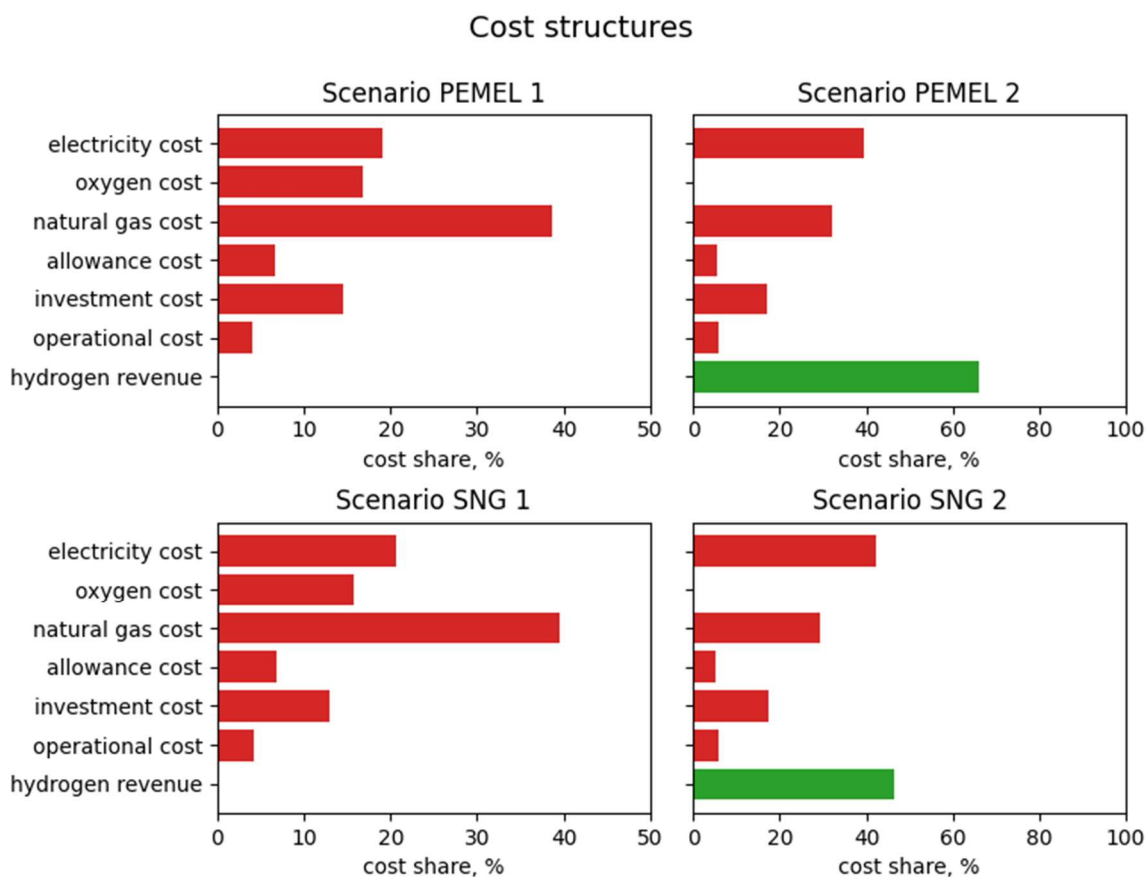


Figure 6-6: Cost structure for future scenarios

As shown in Table 6-3, some of the future scenarios are not profitable using model parameters from 2020. Figure 6-7 illustrates how changes in selected parameters would affect total annual energy costs, thereby possibly presenting a future outlook on scenario performances while also investigating the sensitivity of the energy system model. The total annual energy costs of each scenario are plotted over the currently investigated parameter. All total annual energy costs are thereby given in per cent of the total annual energy cost for the reference scenario. Thick markers represent the total annual energy costs when using the original parameters, while thin markers represent costs calculated by using deviant model parameters. These points were then used to fit the depicted curves. Investigated parameters are the natural gas price, the LOX price, the price for CO₂ emission allowance, the price for selling hydrogen, the electrolyzers specific CAPEX and the electrolyzers efficiency.

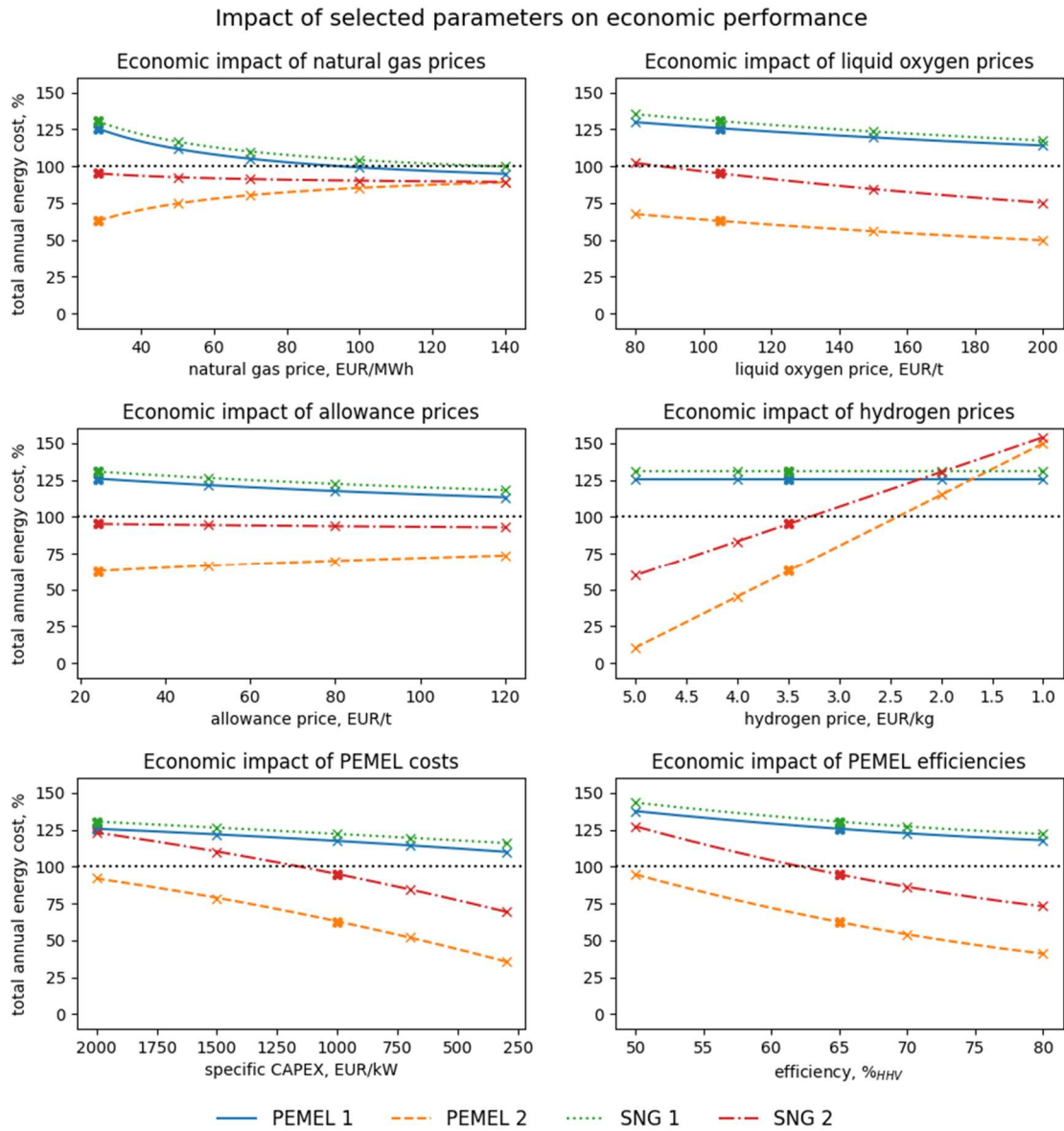


Figure 6-7: Sensitivity of the energy system model to selected parameters

6.3 Discussion

At the beginning of this thesis (see section 2.2), certain objectives were stated in the form of research questions. Now, using the results presented in the above paragraphs, these questions are answered. Moreover, limitations of the applied energy system model are also discussed in this chapter.

6.3.1 Demand side management and emission saving potentials

How does the implementation of PEMEL and methanation technologies affect demand side management and emission saving potentials of an EAF steel mill?

The investigated future scenarios can generally be divided into hydrogen demand-actuated scenarios with comparably low electrolyser capacities and a need for LOX from external suppliers (scenarios PEMEL 1 and SNG 1) and into oxygen demand-actuated scenarios with high electrolyser capacities in the range of 10 MW_{el} and with production of surplus hydrogen for sale (scenarios PEMEL 2 and SNG 2). According to Table 6-2, oxygen demand-actuated scenarios seem to be more flexible and therefore better suited for demand side management, indicated by lower full load hours, lower annual efficiencies and lower mean purchased electricity prices. On the other hand, the hydrogen demand-actuated scenarios PEMEL 1 and SNG 1 run at full load most of the time, thus they are less able to utilize varying electricity prices cost-effectively. This is probably because electrolyser operation in these scenarios is rather limited due to restrictive hydrogen demands. In scenario PEMEL 1, the hydrogen demand is completely predefined and thus electrolysis would not be flexible at all. However, this is countered somewhat by enabling hydrogen storage. In scenario SNG 1, electrolyser operation is not limited by a predefined hydrogen demand, but rather by the inflexibility of the subsequent methanation process.

For assessing the emission saving potentials for the future scenarios, it is assumed that electrolysers only use electricity from CO₂-neutral generation due to demand side management. When only considering CO₂ emissions of the steel mill, scenario PEMEL 2 provides no benefit compared to the reference case, while scenarios PEMEL 1, SNG 1 and SNG 2 substitute natural gas through hydrogen or SNG, thereby reducing the natural gas demand and CO₂ emissions. However, it is assumed that hydrogen sales in scenarios PEMEL 2 and SNG 2 reduce the hydrogen demands of external consumers. Further, it is also assumed that these demands would otherwise be supplied through grey hydrogen. When regarding CO₂ emissions from hydrogen production via SR for such external consumers, scenarios PEMEL 2 and SNG 2 provide a greater emission reduction potential than scenarios PEMEL 1 and SNG 1 (see Table 6-2).

6.3.2 Economic benefits

What economic benefits arise from implementing these technologies and what are the most cost-effective plant layouts and operational strategies?

Concerning the economic viability, the oxygen demand-actuated scenarios PEMEL 2 and SNG 2 have the edge over the other scenarios but also over the reference scenario. In contrast, hydrogen demand-actuated scenarios do not provide an economically feasible alternative to the status quo. The results presented in Table 6-3 and Figure 6-6 seem to indicate that hydrogen utilization is the predominant variable for cost-effective electrolyser operation. Scenarios PEMEL 2 and SNG 2 are profitable mainly due to the high prices for selling hydrogen. When planning the implementation and operation of an electrolyser, the focus should thus be on finding a reliable customer for high-quality hydrogen. In contrast, scenarios PEMEL 1 and SNG 1 use hydrogen only to substitute natural gas, either via hydrogen combustion or via SNG production. Compared to the production costs for hydrogen, natural gas prices are quite low. Therefore, natural gas substitution is not a cost-effective way of hydrogen utilization. This explains also why the total costs in scenario SNG 2 are higher than in scenario PEMEL 2. Valuable hydrogen, that would otherwise generate high revenue from selling, is partially converted to SNG.

As described in chapter 3.4, oxygen from electrolysis should be only viewed as a by-product, owing to the high specific energy demand when compared to conventional methods of oxygen production. By also utilizing by-product oxygen in the steel mill, therefore avoiding or lowering costs for purchasing and transporting LOX, electrolysis is more cost-effective than similar hydrogen production plants where oxygen is wasted. The subplot “Economic impact of hydrogen prices” in Figure 6-7 indicates how low the hydrogen selling price could be set for scenarios PEMEL 2 and SNG 2 to still outperform the reference scenario thanks to simultaneous oxygen and hydrogen utilization.

6.3.3 Sensitivity of the energy system model

What variables have the strongest effects on economic viability?

For scenarios PEMEL 2 and SNG 2, the hydrogen selling price mentioned above has a large effect on the economic viability. However, this thesis also investigated the economic impact of other variables. According to Figure 6-7, scenarios where natural gas is substituted (PEMEL 1, SNG 1 and SNG 2) benefit from increasing natural gas and allowance prices. Scenarios where the complete oxygen demand is covered via electrolysis (PEMEL 2 and SNG 2) are not affected by LOX prices. However, compared to the other scenarios and the reference case, scenarios PEMEL 2 and SNG 2 perform better when LOX prices increase. Moreover, a large cost reduction potential exists for scenarios PEMEL 2 and SNG 2 at decreasing specific

CAPEX or increasing efficiencies for electrolysis units. Because of higher nominal electrolyser capacities and higher hydrogen and oxygen production rates, scenarios PEMEL 2 and SNG 2 are much more affected by these parameters than scenarios PEMEL 1 and SNG 1.

6.3.4 Model limitations

When considering optimization results, it is also important to regard the limitations for the energy system model. For instance, optimization gives the most cost-effective plant layout and operational strategy under the assumption that operators have perfect foresight on electricity price changes. Thus, the optimized operational strategies depicted in this thesis do not represent actual plant operations but rather theoretical cost-saving potentials.

Another limitation is the fact that waste heat flows are not considered in the simplified demand model used for this thesis. Consequently, heat flows are also disregarded in the optimization model. Especially in scenarios SNG 1 and SNG 2, where an exothermic methanation process is implemented, economic benefits from waste heat utilization could be quite significant.

In the present model, fixed prices are applied for natural gas and CO₂ emission allowances throughout the complete optimization time. It would be possible to use variable prices instead, analogous to the price profiles for electric energy. Optimization of the model would then not only aim to minimize electricity costs, but also natural gas costs and allowance costs.

Moreover, an optimization time of only four weeks is used in the energy system model, therefore it is necessary to also pick electricity prices for the same period. It is thus difficult to depict seasonal electricity price changes. There are possible solutions for this problem, for instance, using a mixture of incoherent weeks, each one representing one season. However, for the sake of simplicity, it was decided to use four continuous summer weeks instead. For further optimizations in the future, increasing the optimization time to one year might be of interest. Thus, it would be possible to depict seasonal electricity price changes in the energy system model.

7 CONCLUSION AND OUTLOOK

In view of the upcoming energy transition, PtG-technologies and strategies for demand side management will increase in importance. Implementing an electrolyser to an EAF steel mill would provide demand side flexibility, thereby enabling better integration of CO₂-neutral energy sources into the future electricity grid.

However, only large-scale electrolysers for demand-actuated oxygen production (scenarios PEMEL 2 and SNG 2) should be used. The higher investment costs for such plants are counterbalanced by potential revenues from selling surplus hydrogen. Due to the utilization of by-product oxygen, hydrogen production costs are thereby lower than for comparable electrolysis plants where oxygen is wasted.

In contrast, the annual costs for hydrogen demand-actuated scenarios are higher than for the reference case. These scenarios are thus not economically viable. Only a drastic change in framework conditions (see Figure 6-7) would enable scenarios PEMEL 1 and SNG 1 to outperform the reference scenario. Moreover, due to rather restrictive hydrogen demands, these scenarios provide less demand side flexibility than the oxygen demand-actuated scenarios.

Using prices from 2020, natural gas is much cheaper than hydrogen. Therefore, implementing a methanation plant and converting hydrogen to SNG is not cost-effective when selling hydrogen is an option. However, increasing prices for natural gas and emission allowance as well as decreasing production costs for hydrogen could change this in the future.

After generating results for the year 2020 by using historical data, the next logical step would be to model and optimize upcoming years. Forecasts could be used to generate parameters for these future models, depicting the effect of future electricity price profiles would thereby be of particular interest.

In future optimizations, different oxygen provision methods could be modelled and assessed alongside the utilization of by-product oxygen from PEMEL, for instance, on-site oxygen production via PSA. Because electric energy is necessary for PSA operation, generating oxygen this way would also provide a potential for demand side management.

Regarding the high importance of optimal hydrogen utilization for economic electrolyser operation, it would be also very interesting for the energy system model to include possible hydrogen consumers in a more detailed manner. Instead of just considering hydrogen compression and selling surplus hydrogen for a fixed price, future works could regard the actual hydrogen demands of potential customers.

8 BIBLIOGRAPHY

- [1] EUROFER: *European Steel in Figures 2021*. URL <https://www.eurofer.eu/publications/brochures-booklets-and-factsheets/european-steel-in-figures-2021/> – review date 2022-02-07
- [2] TOKTAROVA, Alla ; KARLSSON, Ida ; ROOTZÉN, Johan ; GÖRANSSON, Lisa ; ODENBERGER, Mikael ; JOHNSON, Filip: *Pathways for Low-Carbon Transition of the Steel Industry—A Swedish Case Study*. In: *Energies* 13 (2020), No. 15, Article 3840.
- [3] QUADER, M. Abdul ; AHMED, Shamsuddin ; GHAZILLA, Raja Ariffin Raja ; AHMED, Shameem ; DAHARI, Mahidzal: *A comprehensive review on energy efficient CO2 breakthrough technologies for sustainable green iron and steel manufacturing*. In: *Renewable and Sustainable Energy Reviews* 50 (2015), S. 594–614
- [4] BUNDESMINISTERIUMS FÜR KLIMASCHUTZ, UMWELT, ENERGIE, MOBILITÄT, INNOVATION UND TECHNOLOGIE: *energy innovation austria : Energiespeicher*. URL <https://www.energy-innovation-austria.at/article/energiespeicher/> – review date 2022-02-07
- [5] GORRE, Jachin ; RUOSS, Fabian ; KARJUNEN, Hannu ; SCHAFFERT, Johannes ; TYNJÄLÄ, Tero: *Cost benefits of optimizing hydrogen storage and methanation capacities for Power-to-Gas plants in dynamic operation*. In: *Applied Energy* 257 (2020), 1–2, Article 113967.
- [6] SCHIEBAHN, Sebastian ; GRUBE, Thomas ; ROBINIUS, Martin ; TIETZE, Vanessa ; KUMAR, Bhunesh ; STOLTEN, Detlef: *Power to gas: Technological overview, systems analysis and economic assessment for a case study in Germany*. In: *International Journal of Hydrogen Energy* 40 (2015), No. 12, S. 4285–4294
- [7] VAN LEEUWEN, Charlotte ; MULDER, Machiel: *Power-to-gas in electricity markets dominated by renewables*. In: *Applied Energy* 232 (2018), S. 258–272
- [8] KATO, Takeyoshi ; KUBOTA, Mitsuhiro ; KOBAYASHI, Noriyuki ; SUZUOKI, Yasuo: *Effective utilization of by-product oxygen from electrolysis hydrogen production*. In: *Energy* 30 (2005), No. 14, S. 2580–2595
- [9] DOCK, Johannes ; JANZ, Daniel ; WEISS, Jakob ; MARSCHNIG, Aaron ; KIENBERGER, Thomas: *Time- and component-resolved energy system model of an electric steel mill*. In: *Cleaner Engineering and Technology* 4 (2021), Article 100223.
- [10] NAPP, T. A. ; GAMBHIR, A. ; HILLS, T. P. ; FLORIN, N. ; FENNELL, P.S: *A review of the technologies, economics and policy instruments for decarbonising energy-intensive*

- manufacturing industries*. In: *Renewable and Sustainable Energy Reviews* 30 (2014), No. 6, S. 616–640
- [11] HASANBEIGI, Ali ; PRICE, Lynn ; ARENS, Marlene: *Emerging Energy-efficiency and Carbon Dioxide Emissions-reduction Technologies for the Iron and Steel Industry* / Ernest Orlando Lawrence Berkeley National Laboratory, Fraunhofer Institute for Systems and Innovation Research (ISI), Energy Foundation and Dow Chemical Company (contract No.DE-AC02-05CH11231). 2013
- [12] HEGEMANN, Karl-Rudolf ; GUDER, Ralf: *Stahlerzeugung*. Wiesbaden : Springer Fachmedien Wiesbaden, 2020
- [13] BAUKAL, Charles E.: *Oxygen-Enhanced Combustion*. 2nd ed. Hoboken : CRC Press, 2013 (Industrial Combustion Series)
- [14] MEDIAS, Jorge: Electric Furnace Steelmaking. In: SEETHARAMAN, Seshadri; MCLEAN, Alex; GUTHRIE, Roderick I. L.; SRIDHAR, Seetharaman (ed.): *Treatise on Process Metallurgy : Volume 3: Industrial Processes, Part A*. Kidlington, Oxford, U.K, Waltham, Mass : Elsevier, 2014, S. 271–300
- [15] ZARANDI, M.H. Fazel ; AHMADPOUR, P.: *Fuzzy agent-based expert system for steel making process*. In: *Expert Systems with Applications* 36 (2009), No. 5, S. 9539–9547
- [16] VON SCHÉELE, Joachim: Oxyfuel combustion in the steel industry : energy efficiency and decrease of CO₂ emissions. In: PALM, Jenny (ed.): *Energy Efficiency*. Rijeka : Sciyo, 2010, S. 83–102
- [17] DONG, Kai ; WANG, Xueliang: *CO₂ Utilization in the Ironmaking and Steelmaking Process*. In: *Metals* 9 (2019), No. 3, Article 273.
- [18] VANSANT, Jan: Carbon Dioxide Emission and Merchant Market in the European Union. In: ARESTA, Michele (ed.): *Carbon dioxide recovery and utilization*. Dordrecht, Netherlands : Springer Science+Business Media, 2003, S. 3–50
- [19] AHN, Min ; CHILAKALA, Ramakrishna ; HAN, Choon ; THENEPALLI, Thriveni: *Removal of Hardness from Water Samples by a Carbonation Process with a Closed Pressure Reactor*. In: *Water* 10 (2018), No. 1, Article 54.
- [20] CARMO, Marcelo ; FRITZ, David L. ; MERGEL, Jürgen ; STOLTEN, Detlef: *A comprehensive review on PEM water electrolysis*. In: *International Journal of Hydrogen Energy* 38 (2013), No. 12, S. 4901–4934
- [21] NIKOLAIDIS, Pavlos ; POULLIKKAS, Andreas: *A comparative overview of hydrogen production processes*. In: *Renewable and Sustainable Energy Reviews* 67 (2017), S. 597–611

- [22] LEMUS, Ricardo Guerrero ; MARTÍNEZ DUART, José Manuel: *Updated hydrogen production costs and parities for conventional and renewable technologies*. In: *International Journal of Hydrogen Energy* 35 (2010), No. 9, S. 3929–3936
- [23] YU, Minli ; WANG, Ke ; VREDENBURG, Harrie: *Insights into low-carbon hydrogen production methods: Green, blue and aqua hydrogen*. In: *International Journal of Hydrogen Energy* 46 (2021), No. 41, S. 21261–21273
- [24] BUTTLER, Alexander ; SPLIETHOFF, Hartmut: *Current status of water electrolysis for energy storage, grid balancing and sector coupling via power-to-gas and power-to-liquids: A review*. In: *Renewable and Sustainable Energy Reviews* 82 (2018), No. 3, S. 2440–2454
- [25] VARELA, Christopher ; MOSTAFA, Mahmoud ; ZONDERVAN, Edwin: *Modeling alkaline water electrolysis for power-to-x applications: A scheduling approach*. In: *International Journal of Hydrogen Energy* 46 (2021), No. 14, S. 9303–9313
- [26] BARBIR, Frano: *PEM electrolysis for production of hydrogen from renewable energy sources*. In: *Solar Energy* 78 (2005), No. 5, S. 661–669
- [27] NGUYEN, T. ; ABDIN, Z. ; HOLM, T. ; MÉRIDA, W.: *Grid-connected hydrogen production via large-scale water electrolysis*. In: *Energy Conversion and Management* 200 (2019), Article 112108.
- [28] KUCKSHINRICHS, Wilhelm ; KETELAER, Thomas ; KOJ, Jan Christian: *Economic Analysis of Improved Alkaline Water Electrolysis*. In: *Frontiers in Energy Research* 5 (2017), Article 1.
- [29] RÖNSCH, Stefan ; SCHNEIDER, Jens ; MATTHISCHKE, Steffi ; SCHLÜTER, Michael ; GÖTZ, Manuel ; LEFEBVRE, Jonathan ; PRABHAKARAN, Praseeth ; BAJOHR, Siegfried: *Review on methanation – From fundamentals to current projects*. In: *Fuel* 166 (2016), S. 276–296
- [30] MUTZ, Benjamin ; CARVALHO, Hudson W.P. ; MANGOLD, Stefan ; KLEIST, Wolfgang ; GRUNWALDT, Jan-Dierk: *Methanation of CO₂: Structural response of a Ni-based catalyst under fluctuating reaction conditions unraveled by operando spectroscopy*. In: *Journal of Catalysis* 327 (2015), S. 48–53
- [31] SPECHT, Michael ; BRELLOCHS, Jochen ; FRICK, Volkmar ; STÜRMER, Bernd ; ZUBERBÜHLER, Ulrich: *The Power to Gas Process : Storage of Renewable Energy in the Natural Gas Grid via Fixed Bed Methanation of CO₂/H₂*. In: BIOLLAZ, Serge M.; SCHILDHAUER, Tilman J. (ed.): *Synthetic natural gas from coal, dry biomass, and power-to-gas applications*. Hoboken, New Jersey : Wiley, 2016, S. 191–220
- [32] GITHUB: *Open Energy Modelling Framework (oemof)*. URL <https://github.com/oemof/oemof> – review date 2022-02-24

- [33] OEMOF DEVELOPER GROUP: *User's guide*. URL <https://oemof-solph.readthedocs.io/en/latest/usage.html> – review date 2022-02-24
- [34] GAO, Ming ; KRISHNAMURTHY, Ravi: Hydrogen Transmission in Pipelines and Storage in Pressurized and Cryogenic Tanks. In: GUPTA, Ram B. (ed.): *Hydrogen fuel : Production, transport, and storage*. Boca Raton : CRC Press, 2009, S. 341–407
- [35] AUSTRIAN POWER GRID AG: *EXAA day-ahead Preise*. URL <https://www.apg.at/de/markt/Markttransparenz/Uebertragung/EXAA-Spotmarkt> – review date 2022-03-10
- [36] E-CONTROL: *Preisentwicklung Strom*. URL <https://www.e-control.at/statistik/strom/marktstatistik/preisentwicklung> – review date 2022-01-24
- [37] BUNDESREPUBLIK ÖSTERREICH. ElWOG (2010-02-01) § 111 para. 3
- [38] PETERS, Max Stone ; TIMMERHAUS, Klaus D. ; WEST, Ronald E.: *Plant design and economics for chemical engineers*. 5th ed. New York : McGraw-Hill, 2003 (McGraw-Hill chemical engineering series)
- [39] HANAK, Dawid P. ; POWELL, Dante ; MANOVIC, Vasilije: *Techno-economic analysis of oxy-combustion coal-fired power plant with cryogenic oxygen storage*. In: *Applied Energy* 191 (2017), S. 193–203
- [40] HU, Yukun ; LI, Xun ; LI, Hailong ; YAN, Jinyue: *Peak and off-peak operations of the air separation unit in oxy-coal combustion power generation systems*. In: *Applied Energy* 112 (2013), No. 1, S. 747–754
- [41] E-CONTROL: *Preisentwicklung Gas*. URL <https://www.e-control.at/statistik/gas/marktstatistik/preisentwicklung> – review date 2022-01-24
- [42] EUROPEAN ENERGY EXCHANGE AG: *Emission Spot Primary Market Auction Report 2022*. URL <https://www.eex.com/en/market-data/environmental-markets/eua-primary-auction-spot-download> – review date 2022-01-24
- [43] ŠULC, Radek ; DITL, Pavel: *A technical and economic evaluation of two different oxygen sources for a small oxy-combustion unit*. In: *Journal of Cleaner Production* 309 (2021), Article 127427.
- [44] GREIML, Matthias ; FRITZ, Florian ; KIENBERGER, Thomas: *Increasing installable photovoltaic power by implementing power-to-gas as electricity grid relief – A techno-economic assessment*. In: *Energy* (2021), No. 235, Article 121307.

- [45] MURADOV, Nazim: *Hydrogen via methane decomposition : an application for decarbonization of fossil fuels*. In: *International Journal of Hydrogen Energy* 26 (2001), S. 1165–1175
- [46] EUROSTAT: *Producer prices in industry, domestic market -monthly data*. URL https://appsso.eurostat.ec.europa.eu/nui/show.do?dataset=sts_inppd_m&lang=en – review date 2022-02-22
- [47] CHEMICAL ENGINEERING: *The chemical engineering plant cost index*. URL <https://www.chemengonline.com/pci-home> – review date 2022-02-22
- [48] TURTON, Richard: *Analysis, synthesis, and design of chemical processes*. 5th ed. Boston : Prentice Hall, 2018 (Prentice Hall international series in the physical and chemical engineering sciences)
- [49] EUROPEAN CENTRAL BANK: *Euro foreign exchange reference rates*. URL https://www.ecb.europa.eu/stats/policy_and_exchange_rates/euro_reference_exchange_rates/html/eurofxref-graph-usd.en.html – review date 2022-02-22

9 APPENDIX

The first part of the appendix describes the methodology for comparing monetary values from different years. The second section contains the figures for electricity utilization in the future scenarios.

9.1 Cost indices

Throughout this thesis, monetary values need to be adjusted to EUR in the year 2020 to make them comparable. This is accomplished by using the cost indices shown in Table 9-1. For investment costs, the chemical engineering plant cost index (CEPCI) is used, while hydrogen production costs and natural gas prices are adjusted with the EU producer price index (PPI). PPIs stem from [46] and CEPCIs are obtained from [47] and [48].

Table 9-1: Cost indices for plant costs and production costs

Year	2005	2009	2013	2015	2017	2018	2020
CEPCI	468	521	567	557	567.5	603.1	596.2
PPI	83.7	93.3	105.1	100.0	101.7	105.3	102.8

Such indices show the cost at a given time relative to a defined base time. For instance, 2015 is the base time for the PPI, indicated by a value of 100. By using equation (9-1), original costs obtained from some moment b in the past can be updated to represent costs at time a with the help of the respective indices [38]. Cost values in USD are then converted to EUR using the average exchange rate of 1.142 \$/EUR for the year 2020 [49].

$$cost_{time\ a} = cost_{time\ b} * \left(\frac{index_{time\ a}}{index_{time\ b}} \right) \quad (9-1)$$

9.2 Electricity utilization

As mentioned in chapter 6.1, all figures showing the electricity utilization in future scenarios are presented below. The top subplots show the current electricity price for PEMEL operation in EUR/MWh_{el}, the bottom subplots illustrate the power consumption for electrolysis in kW_{el}. Electricity price and power consumption are both plotted over time in days. All plots depict thereby the first week of the four weeks spanning optimization time.

Power consumption PEMEL 1

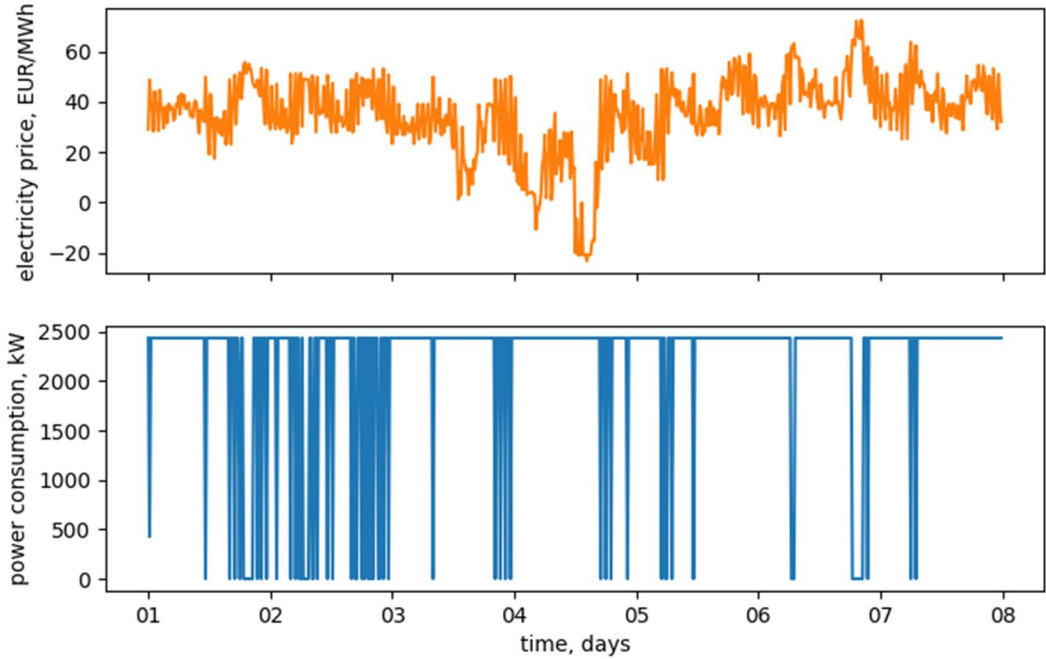


Figure 9-1: Electricity utilization in scenario PEMEL 1

Power consumption PEMEL 2

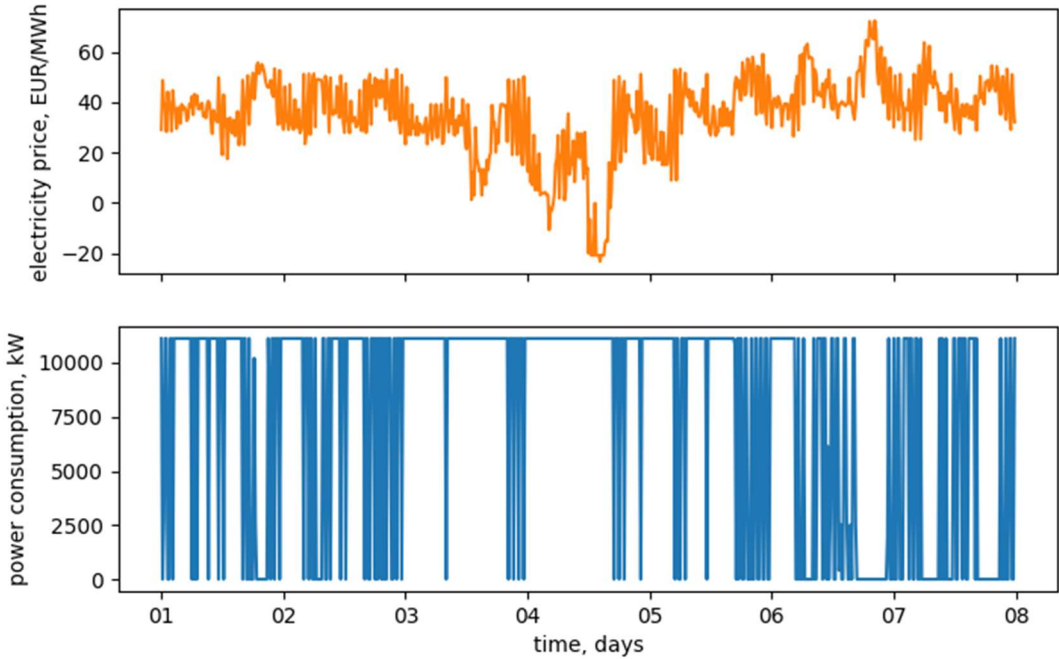


Figure 9-2: Electricity utilization in scenario PEMEL 2

Power consumption SNG 1

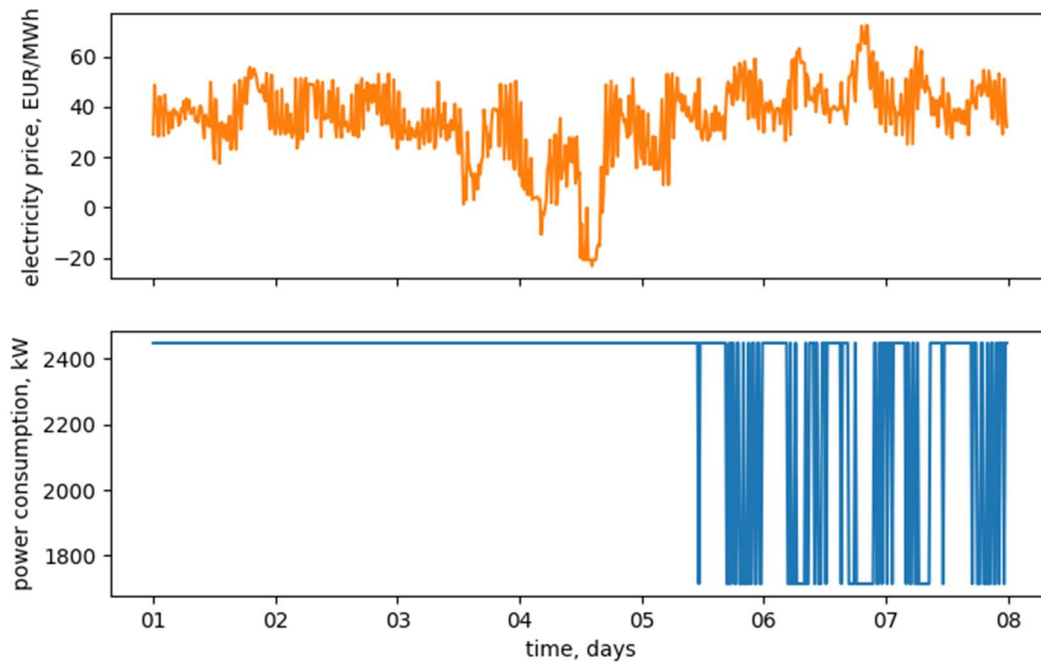


Figure 9-3: Electricity utilization in scenario SNG 1

Power consumption SNG 2

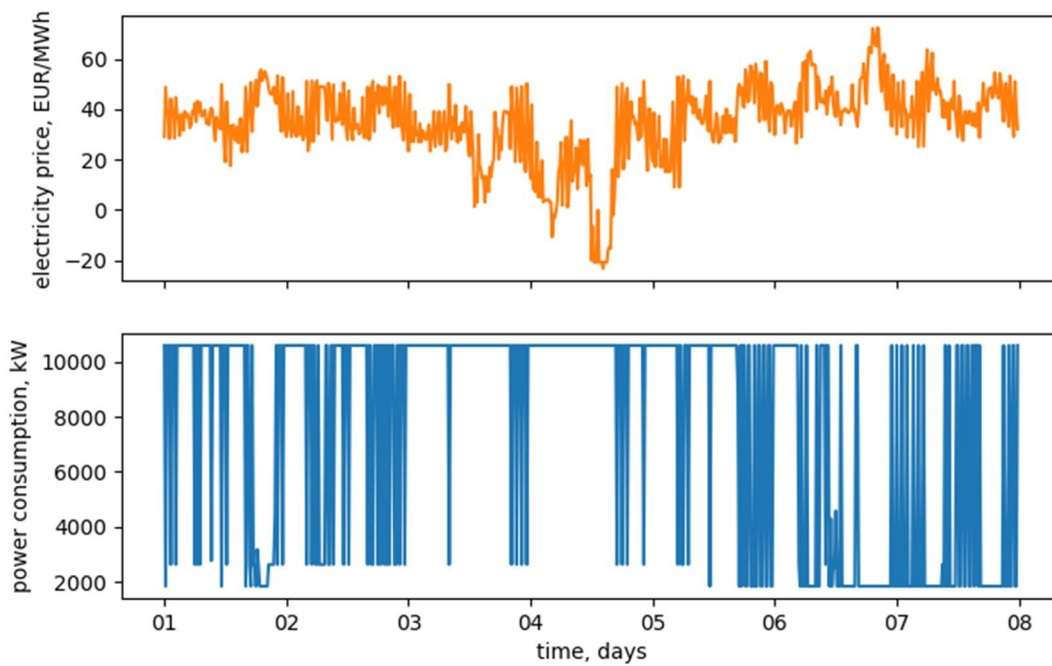


Figure 9-4: Electricity utilization in scenario SNG 2